UNIVERSIDADE DE LISBOA
FACULDADE DE CIÊNCIAS
DEPARTAMENTO DE BIOLOGIA VEGETAL

Development and characterization of an innovative drug delivery platform targeting breast cancer brain metastases

Joana Raquel Aniceto Romão

Mestrado em Biologia Molecular e Genética

Dissertação orientada por:
Prof. ª Dra. Maria Alexandra Brito (abrito@ff.ulisboa.pt)
Prof. Dr. Rui Malhó (rmmalho@fc.ul.pt)

2022

The studies present in this master thesis were performed in the research groups "Neurovascular Lab" and "Advanced Technologies for Drug Delivery Lab", from the Research Institute for Medecines (iMed.ULisboa), Faculty oh Pharmacy, Universidade de Lisboa, under the supervision of Professor Doctor Maria Alexandra Brito and Professor Rui Malhó.

This work was supported by Fundação para a Ciência e Tecnologia (FCT-PTD/MED-ONC/29402/2017 and UIDB/04138/2020)

Outputs ensuing from the present thesis

Publications in scientific journals

Aniceto-Romão J*, Godinho-Pereira J*, Malhó R, Mendonça LS, Silva AB, Corvo ML, Jurado A, Pedroso de Lima CM, Bronze R, Duarte N, Carvalheiro M, Brito MA. Development and characterization of chlorotoxin functionalized nanomedicines encapsulating salinomycin and small interfering platelet-derived growth factor B: A innovative approach for the abrogation of breast cancer brain metastasis (In preparation)

Godinho-Pereira J*, Vaz D*, Aniceto-Romão J, Gaspar MM, Rocha J, Malhó R, Simões S, Carvalheiro MC, Brito MA. Implementation and characterization of an *in vivo* model of breast cancer brain metastases. (In preparation)

Godinho-Pereira J, Silvestre R, Vaz D, Aniceto-Romão J, Malhó R, Gaspar MM, Simões S, Corvo ML, Carvalheiro MC, Brito MA. A new preventive therapeutic targeting the blood-brain barrier: averting breast cancer brain metastases development by a minocycline hydrochloride loaded nanomedicine. (In preparation)

Publications in abstract books

Aniceto-Romão J, Godinho-Pereira J, Malhó R, Mendonça LS, Corvo M.L, Jurado A, Pedroso de Lima CM, Carvalheiro M, Brito MA. A new nanomedicine platform targeting breast cancer brain metastases to silence platelet-derived growth factor B. 13th iMed.ULisboa Posgraduate Studenst Meeting, Lisbon, Portugal, July 4th- 5th 2022

Aniceto-Romão J, Godinho-Pereira J, Malhó R, Mendonça LS, Corvo ML, Pedroso de Lima C, Carvalheiro C, Brito MA. Targeting breast cancer brain metastases by blood-brain barrier-permeant drug delivery system to silence platelet-derived growth factor B. Innovate competition iMED Conference 14.0, Lisbon, Portugal, October 12th-16th 2022.

Posters

Aniceto-Romão J, Godinho-Pereira J, Malhó R, Mendonça LS, Corvo M.L, Jurado A, Pedroso de Lima CM, Carvalheiro M, Brito MA. A new nanomedicine platform targeting breast cancer brain metastases to silence platelet-derived growth factor B. 13th iMed.ULisboa Posgraduate Studenst Meeting, Lisbon, Portugal, July 4th- 5th 2022

Aniceto-Romão J, Godinho-Pereira J, Malhó R, Mendonça LS, Corvo ML, Pedroso de Lima C, Carvalheiro C, Brito MA. Targeting breast cancer brain metastases by blood-brain barrier-permeant drug delivery system to silence platelet-derived growth factor B. Innovate competition iMED Conference 14.0, Lisbon, Portugal, October 12th-16th 2022.

Pitch Communications

Aniceto-Romão J, Godinho-Pereira J, Malhó R, Mendonça LS, Corvo ML, Pedroso de Lima C, Carvalheiro C, Brito MA. Targeting breast cancer brain metastases by blood-brain barrier-permeant drug delivery system to silence platelet-derived growth factor B. Innovate competition iMED Conference 14.0, Lisbon, Portugal, October 12th-16th 2022.

Acknowledgements / Agradecimentos

Em primeiro lugar gostaria de agradecer à minha orientadora, Professora Maria Alexandra Brito, por me ter recebido no Neurovascular Lab e por me ter dado a oportunidade de descobrir o que é a investigação, muitas vezes "90% de transpiração e 10% de criação". Gostaria de agradecer também por ter contribuído para o meu crescimento científico e pessoal, e por toda a ajuda demonstrada ao logo deste ano desafiante.

De seguida, gostaria de agradecer ao Professor Rui Malhó, por aceitar ser meu orientador interno, pela disponibilidade cedida e pela rápida resposta sempre que necessário. Gostaria de agradecer também pela disponibilização de todos os equipamentos de microscopia necessários para o desenvolvimento deste trabalho.

Não posso deixar de agradecer à Doutora Manuela Colla, sem ela este trabalho não seria possível. Apesar de não ser minha orientadora, sempre se demonstrou disponível para me ajudar em tudo o que fosse necessário, mesmo que isso implicasse "puxar uma cadeira" e trabalharmos lado a lado. Obrigada por todas as horas dispensadas a discutirmos trabalho pelas horas a fora.

Gostaria de agradecer à Professora Maria do Rosário Bronze, à Professora Noélia Duarte e à Doutora Andreia Bento da Silva por toda a ajuda disponibilizada na quantificação da Salinomicina. Gostaria de agradecer ainda à Professora Conceição Pedroso de Lima, à Professora Amélia Jurado e a Doutora Liliana Mendoça por toda a ajuda e informação dada no desenvolvimento da nanoformulação.

Queria agradecer também a todos os membros do grupo do Neurovascular Lab. Em primeiro lugar, obrigada por tudo Joana, não há palavras suficientes para agradecer tudo o que fizeste por mim ao longo deste ano. Ajudas-te sempre em tudo o que precisei mesmo nos meus mini ataques, incentivaste-me a acreditar em mim e a crescer enquanto cientista. Espero que não te esqueças das nossas conversas à "Joanas" que só nos percebemos. Este ano não seria o mesmo sem ti. Queria agradecer também à Rita por toda a ajuda que me deste ao longo deste ano e principalmente pelo "Oh Rita" com direito a entrada sorrateira. Quero agradecer à Catarina e à Daniela, que começaram estas jornada ao mesmo tempo que eu. Catarina obrigada por seres a minha 2ª/4ª opinião, pelas horas que te fiz passar no fluxo quando tinha de ir para o Lumiar e obrigada também pelas histórias da terrinha. Daniela obrigada pela companhia, por toda a ajuda e por todas as risadas ao logo deste ano e continua a ser "especial". Às meninas novas, Rute e Beatriz, obrigada por toda a ajuda que me deram ao longo deste curto tempo e desejo-vos a maior sorte para este próximo ano. Por último, obrigada à Sara e à Rafaela por toda a ajuda que me deram no início deste percurso e sempre que precisei.

Não podia deixar de agradecer às minhas Marias. Jéssica, obrigada pela paciência e por estares sempre lá quando precisei, nem que fosse para um almoço rápido. Inês, a minha companheira de chamadas de telemóvel ao fim da tarde. Obrigada por estares lá sempre à distância de uma chamada ou via zoom e por todos os conselhos e sugestões que enriqueceram esta etapa.

Por último, mas não menos importante quero agradecer à minha família por todo o apoio neste ano tão diferente. Principalmente aos meus pais e à minha irmã, que levaram com o meu mau humor e cansaço quando chegava a casa. Mas estiveram lá sempre para me apoiar dar força para continuar e que no final conseguiram ver o meu sucesso.

Abstract

15-25 % of breast cancer (BC) patients develop brain metastases (BM), a poor prognosis condition due to the restricted blood-brain barrier (BBB) permeability. Platelet-derived growth factor subunit B (PDGF-B) was associated with BC cells (BCCs) proliferation. Furthermore, salinomycin (SAL) was effective in the eradication of BCCs. Nanoformulations coupled to chlorotoxin (CTX), appear as a strategy to overcome the BBB and achieve target-specific delivery. This prompted us to develop a new nanomedicines platform decorated with CTX for combined drug (SAL) and genetic (siRNA) therapeutic approach to abrogate BC brain metastases (BCBM).

Liposomes with siPDGF-B were developed and their biological activity towards triple negative BCCs (4T1 cells) was determined based on cell viability and PDGF-B silencing. SAL incorporation was optimized, and characterized, and SAL encapsulated median lethal dose (LD50) was determined. The efficiency of co-administration was studied based on cell viability, PDGF-B silencing, and proliferation. The safety of both formulations for brain microvascular endothelial cells (b.End5 cells) was studied. BBB transposition efficiency, and efficacy to abrogate BCCs were evaluated in a co-culture model. Finally, the BBB integrity was ensured by transendothelial electrical resistance (TEER) and the β-catenin labeling.

siPDGF-B presented no effect on 4T1 cells' viability, while PDGF-B silencing efficacy achieved 31%. SAL showed around 33% SAL incorporation efficiency, achieving a LD50 of 24.76 µM. Moreover, co-administration treatment modulated 4T1 cells' proliferation. Importantly, both formulations showed no effect on b.End5 cells' viability. Using the co-culture model, liposomes' ability to act on BCCs, decreasing PDGF-B expression was demonstrated. Additionally, liposomes individually lead to cell senescence. Lastly, TEER and β-catenin labeling revealed b.End5 monolayer disruption by SAL.

Overall, the delivery of SAL appears to impair the endothelium, while siPDGF-B delivery in a targeted and BBB-permeant platform emerges as a new approach for BCBM treatment.

Keywords: breast cancer brain metastases, blood-brain barrier, liposome, platelet-derived growth factor B, salinomycin

Resumo

O cancro da mama afeta mais de 2 milhões de mulheres todos os anos e causa mais de 600 000 mortes. Dentro dos diferentes tipos de cancro da mama, o triplo negativo é o mais agressivo e um dos que apresenta uma maior taxa de formação de metástases encefálicas. Aliado a este fato, é também o que tem menos opções terapêuticas, devido à falta de recetores específicos, o que impossibilita uma terapia direcionada levando assim a uma diminuição na qualidade de vida e na sobrevida destes doentes. Quando diagnosticadas as metástases encefálicas, os pacientes têm em média menos de 1 ano de vida, sendo que apenas 20% sobrevivem até 1 ano. Além disso, a permeabilidade restrita da barreira hematoencefálica torna o tratamento atual de pacientes com metástases encefálicas ineficaz. Portanto, o desenvolvimento de novas abordagens terapêuticas e/ou genéticas para o tratamento de metástases encefálicas associadas ao cancro da mama triplo negativo é uma necessidade não atendida e que carece de maiores esforços de investigação. A subunidade B do fator de crescimento derivado de plaquetas (PDGF-B) demonstrou estar envolvida na proliferação precoce e sustentada de células de cancro da mama, o que indica que o silenciamento da sua expressão pode ser útil para a redução de metástases encefálicas. Além do mais, a salinomicina (SAL) tem-se mostrado um fármaco eficaz na erradicação de células tumorais, o que sugere que possa ser benéfica no tratamento de metástases encefálicas de cancro da mama. No entanto, devido à diminuta permeabilidade da barreira hematoencefálica, sistemas de transporte capazes de transpô-la, assim como nanoformulações, aparentam ser relevantes para veicular fármacos e ácidos nucleicos ao encéfalo. O acoplamento dessas partículas a peptídeos, como a clorotoxina (CTX), permite o seu direcionamento para as células de interesse e reduz a sua toxicidade colateral. A fim de desenvolver e estudar a eficiência de um novo tratamento, tivemos como objetivo desenvolver uma nova plataforma de nanomedicamentos decorada com CTX para uma abordagem terapêutica que combina um fármaco (SAL) e genética (siRNA) com o propósito de diminuir ou eliminar as metástases encefálicas. Para chegar ao objetivo várias tarefas foram definidas: 1) avaliar o efeito do silenciamento de PDGF-B na viabilidade celular, bem como a sua expressão; 2) estudar a eficiente encapsulação de SAL num lipossoma; 3) avaliar a capacidade de SAL incorporada em afetar a viabilidade celular, bem como determinar a dose letal média (DL50) da SAL livre e incorporada; 4) avaliar o efeito da terapia combinada na viabilidade celular, expressão de PDGF-B e proliferação celular: 5) garantir a segurança de cada uma das formulações no que diz respeito à viabilidade das células endoteliais; 6) e por último, avaliar a eficácia dos lipossomas para transpor a barreira hematoencefálica e atuar sobre as células tumorais, monitorizando a integridade da barreira hematoencefálica pela medição da resistência elétrica transendotelial (TEER) e pela análise da expressão da proteína de adesão β-catenina.

Anteriormente no Laboratório Neurovascular, foram desenvolvidas partículas lipídicas de ácido nucleico estáveis (SNALPs) acopladas a CTX que encapsulavam siPDGF-B (CTX-siPDGF-B-SNALPs) pelo método de injeção de etanol. Neste trabalho a sua atividade biológica em células de cancro da mama triplo negativo (linha celular 4T1) foi determinada com base na análise da viabilidade celular (teste de Resazurina) e silenciamento de PDGF-B (PCR quantitativo de transcriptase reversa, RT-qPCR). Em seguida, foram desenvolvidos lipossomas acoplados a CTX que incorporavam SAL (CTX-SAL-Lip), e foram caracterizadas as suas propriedades físico-químicas. Foi determinada a DL50 da SAL pelo ensaio de viabilidade celular (teste da Resazurina). Foi estudada a eficiência da coadministração de siPDGF-B e SAL incorporada com base na análise na viabilidade celular e expressão de PDGF-B (RT-qPCR). Foi também estudado o efeito de CTX-siPDGF-B-SNALPs e CTX-SAL-Lip na proliferação celular através da expressão do marcador de proliferação Ki-67. A segurança para células endoteliais microvasculares do cérebro (linha celular b.End5) foi estudada após o tratamento com CTX-siPDGF-B-SNALPs e CTX-SAL-Lip. Foram ainda avaliadas a integridade da barreira hematoencefálica, a eficiência de transposição e a eficácia para diminuir células de cancro da mama

num modelo de co-cultura de células 4T1 e b.End5 que mimetizam metástases encefálicas do cancro da mama. A eficácia na transposição da barreira hematoencefálica e efeito nas células malignas foi avaliada pela expressão de PDGF-B nas células 4T1. Foi ainda estudada a senescência celular com base na análise da expressão de p16 (RT-qPCR). Finalmente, a integridade da barreira hematoencefálica foi monitorizada pela medição da TEER e pela análise da marcação da β-catenina (imunofluorescência).
Nas concentrações de siRNA estudadas, os CTX-siPDGF-B-SNALPs não comprometeram a viabilidade das células 4T1, tendo a eficácia de silenciamento de PDGF-B atingido 27% com 10 nM e 31% com 50 nM de siPDGF-B. Sendo assim, a concentração de 50 nM foi escolhida para prosseguir com os estudos. De seguida a eficiência de incorporação de SAL num lipossoma com siRNA foi estudada, demonstrando que a co-encapsulação não era possível. Várias tentativas de desenvolver um lipossoma que incorporava apenas SAL foram estudadas, chegando a formulação final com um tamanho médio de 163 nm, carga neutra, e cerca de 33% de eficiência de incorporação da SAL. A DL50 da SAL incorporada atingiu o valor de 24,76 µM, 5x superior à SAL livre. A coadministração de CTX-siPDGF-B e CTX-SAL-Lip não demonstrou diminuir a expressão de PDGF-B em comparação com os lipossomas apenas com siPDGF-B ou SAL. No estudo da proliferação celular, foi possível determinar que o lipossoma com SAL provoca um efeito superior ao lipossoma com siPDGF-B na diminuição de células Ki-67 positivas. Demonstramos ainda que a coadministração de CTX-siPDGF-B-SNALPs e CTX-SAL-Lip leva a um aumento de efeito na diminuição da proliferação de células 4T1 quando comparado com lipossomas apenas com siPDGF-B e SAL. De forma a perceber o impacto dos tratamentos e garantir a segurança para as células endoteliais, tanto CTX-siPDGF-B-SNALPs como CTX-SAL-Lip foram testados nas b.End5 não demonstrando qualquer efeito na sua viabilidade. Com o modelo de co-cultura, demonstrámos a capacidade de CTX-siPDGF-B-SNALPs e CTX-SAL-Lip em transpor a barreira hematoencefálica e atuar nas células de cancro da mama, diminuindo a expressão de PDGF-B. Mais ainda, pelo aumento de p16, demonstrámos que lipossomas com siPDGF-B ou SAL promovem a senescência das células malignas, mas que a coadministração não leva ao aumento de p16 em comparação com os lipossomas individuais. Por último, pela avaliação da TEER foi possível inferir que os CTX-siPDGF-B-SNALPs não afetavam a integridade da barreira hematoencefálica, enquanto os CTX-SAL-Lip provocavam uma diminuição em cerca de 20% na TEER, que não atingiu a significância estatística. Estes resultados levaram à análise da expressão da β-catenina por imunocitoquímica. Esta análise revelou que o tratamento com CTX-siPDGF-B-SNALPs não induziu alterações, mas que a exposição a lipossomas com SAL levou a uma deslocalização da proteína com acumulação na região perinuclear e à criação de "buracos" na membrana, definidos pela ausência de marcação e/ou expressão da proteína.
Coletivamente, este trabalho demonstra que a veiculação de PDGF-B ou de SAL em plataformas direcionadas para as células malignas e com capacidade de atravessar a barreira hematoencefálica é eficaz na modulação de propriedades tumorais. Revelou também que a veiculação de SAL aparenta ser prejudicial para as células endoteliais, enquanto a de siPDGF-B surge como uma abordagem nova e segura para o combate às metástases encefálicas de cancro da mama. Esta terapia, uma vez confirmada *in vivo*, pode levar a um avanço extraordinário na área da neuro-oncologia, aumentar a esperança média de vida e ainda criar uma esperança na qualidade de vida dos pacientes com metástases encefálicas do cancro da mama.

Palavras-chave: metástases encefálicas do cancro da mama, barreira hematoencefálica, lipossoma, fator de crescimento derivado de plaquetas, salinomicina

Contents

List of Table

List of Figure

Abbreviations

ABC	ATP-binding cassette
BBB	Blood-brain barrier
BC	Breast cancer
BCA	Bicinchoninic acid
BCCs	Breast cancer cells
BCBM	Breast cancer brain metastases
BM	Brain metastases
BMECs	Brain microvascular endothelial cells
BRAC1	Breast cancer gene 1
BSA	Bovine Serum Albumin
Cer16-PEG200	N-palmitoyl-sphingosine-1-[succinyl(methoxypolyethylene glycol) 2000]
CNS	Central nervous system
Chol	Cholesterol
CSC	Cancer stem cells
CTX	Chlorotoxin
CTX-SAL-Lip	Liposome decorated with CTX encapsulating SAL
CTX-siPDGF-B-SNALPs	SNALP decorated with CTX encapsulating siPDGF-B
DMEM	Dulbecco's Modified Eagle Medium
DODAP	1,2-dioleoyl-3-dimethylammonium propane
DOX	Doxorubicin
DPX	Dibutylphthalate Polystyrene Xylene
DRV	Dehydration–Rehydration Method
DSPC	Distearoylphosphatidylcholine
DSPE-PEG	Distearoyl-glycerophosphorylethanolamine–poly(ethyleneglycol)2000
DSPE-PEG-MAL	1,2-distearoyl-sn-glycero-3-phospatidylethanolamine-N-[maleimide (polyethylene glycol)-2000] ammonium salt
E-cadherin	Epithelial-cadherin
ECM	Extracellular matrix
EMT	Epithelial-mesenchymal transition
EPC	Egg phosphatidylcholine

ER	Estrogen receptor
FBS	Fetal Bovine serum
GAPDH	Housekeeping gene glyceraldehyde 3-phosphate dehydrogenase
HBV	Hepatitis B virus
HER	Human epidermal growth factor receptor
IC	Insertion Capacity
IE	Incorporation Efficiency
iRNAs	Interfering RNAs
LD	Loading Capacity
LD50	Median lethal dose
MET	Mesenchymal-epithelial transition
MMP-2	Matrix metalloproteinase-2
mRNA	Messenger RNA
NFs	Nanoformulation
PBS	Phosphate-bufferd saline
PDGF-B	Platelet-derived growth factor B subunit
PdI	Polydispersity index
PFA	Paraformaldehyde
PR	Progesterone receptor
PEG	Polyethylene glycol
RPMI	Roswell Park Memorial Institute Medium
RT	Room Temperature
SAL	Salinomycin
siRNA	Small interfering RNA
SNALPs	Stable nucleic acid lipid particles
STAT3	Signal transducer and activator of transcription 3
TEER	Transendotelial electrical resistance
TNBC	Triple negative breast cancer
UHPLC-MS/MS	Liquid chromatography coupled to a mass spectrophotometer

I. Introduction

The introduction of this dissertation is divided into 4 parts. The first part is entitled "Breast cancer brain metastases", which provides an overview of breast cancer, as well as the formation of brain metastases. The second part describes the influence of a growth factor on the tumor microenvironment entitled "Platelet-derived growth factor subunit B as an influencer on cancer cell tumorigenesis". The third part called "Central nervous system: a big challenge for small interfering RNA delivery" addresses the characteristics of liposomes as delivery systems. Finally, the section "Salinomycin as a potential new drug for brain metastasis treatment" details the characteristics of a cytotoxic drug and the benefits of its incorporation in liposomes.

1.1 Breast cancer brain metastases

Breast cancer (BC) is one of the main neoplastic diseases in woman with an incidence of more than 2 million new cases and more than 680 000 deaths estimated in 2020 [1]. This type of cancer is derived from the epithelial cells in the mammary ducts and can divide into invasive and non-invasive BC. In invasive BC, cancer cells spread outside the basement membrane of ducts affecting the surrounding normal tissue and forming metastases [2].

Regardless of whether it is invasive or non-invasive, BC is a heterogeneous disease that presents different histological and biological characteristics, clinical presentations, behaviors, and responses to therapy [3]. This heterogeneity among BC patients is what allows for the classification into different subtypes. The most used classification to distinguish the different types of BC is based on the expression of surface receptors: the estrogen receptor (ER), the progesterone receptor (PR), and the human epidermal growth factor receptor (HER) 2 [4] and is divided into 3 subtypes [3, 5, 6]. The first subtype is the hormone receptor-positive, which is characterized by the positive expression of ER and/or PR. The second is HER2-positive BC, as the name implies, the HER2 is overexpressed. The last one is triple negative BC (TNBC), which is characterized by the absence of ER, PR, and HER2 expression [5, 6] and by the increased development of metastases [7]. This type constitutes 12–24% of BCs and is the most aggressive cancer among the different types [8]. Normally, TNBC is more frequent in individuals with mutated breast cancer gene 1 (BRCA1) and tumor protein 53 gene and have a worse prognosis, high grade, and do not respond to hormone therapy compared to hormone receptors positive tumors [4, 6].

Although the application of the recognized therapeutic options such as surgery, radiotherapy, chemotherapy, immunotherapy, and targeted therapies have increased the survival of patients with BC in early stages by 30%, some tumor cells manage to escape and lead to the formation of metastases in different and distant organs [2, 9]. About 15-25% of BC patients form brain metastases (BM) [10], accounting to a poor prognosis and decreased quality of life [11, 12]. On average, more than 70% of women with TNBC metastases have an average life expectancy of fewer than 5 years after diagnosis, with almost all of them dying from the disease even with the application of the traditional treatments [13]. Underlying heterogeneity between and within BM, clonally selected molecular differences concerning primary tumor site, as well as the lack of specific receptors that preclude a targeted therapy, are likely contributing factors underlying the ineffectiveness of applied therapies, and the low survival rate [6, 14-16]. In addition to that, factors such as the reduced permeability of the blood-brain barrier (BBB), prevents the passage of most chemotherapeutic agents, which, contribute to the poor prognosis of TNBC metastasis in the central nervous system (CNS) [5, 17].

1.1.1 From primary tumor to brain metastases

In this line, studies have shown that the HER2 and TNBC subtypes have a higher incidence of BM [10]. Metastases are formed through a complex process called metastatic cascade that involves various steps, namely (1) invasion; (2) intravasation; (3) survival; (4) extravasation; and (5) organ colonization [5, 15], as represented in the **Figure 1.1**. The first step is the invasion that comprises the exit of BC cells (BCCs) from the breast ducts to invade the surrounding tissue. This step is dependent on the epithelial-mesenchymal transition (EMT), which consists of the acquisition of mesenchymal characteristics, such as loss of cell-cell interaction and absence of apical-basal polarity, allowing mesenchymal cells to have greater invasiveness than epithelial cells; followed by intravasation, which consists of the entry of BCCs into the bloodstream after separation from the primary tumor [5, 15]. After entering the bloodstream, cancer cells must go through a crucial step which is to survive inside the vessels to the challenges such as shear stress and the attack of immune system cells. BCCs with high brain metastatic potential survive and are directed to the brain, a process also called as homing [5, 15]. The next step is the extravasation into the brain through the BBB, which involves rolling (transient interaction with the microvascular endothelial cells of the brain), firm adhesion, and transendothelial migration (via paracellular and/or transcellular pathways). After entering the brain, cancer cells undergo a mesenchymal-epithelial transition (MET) and regain their epithelial phenotype, contributing to colonization and metastasis development [5, 15].

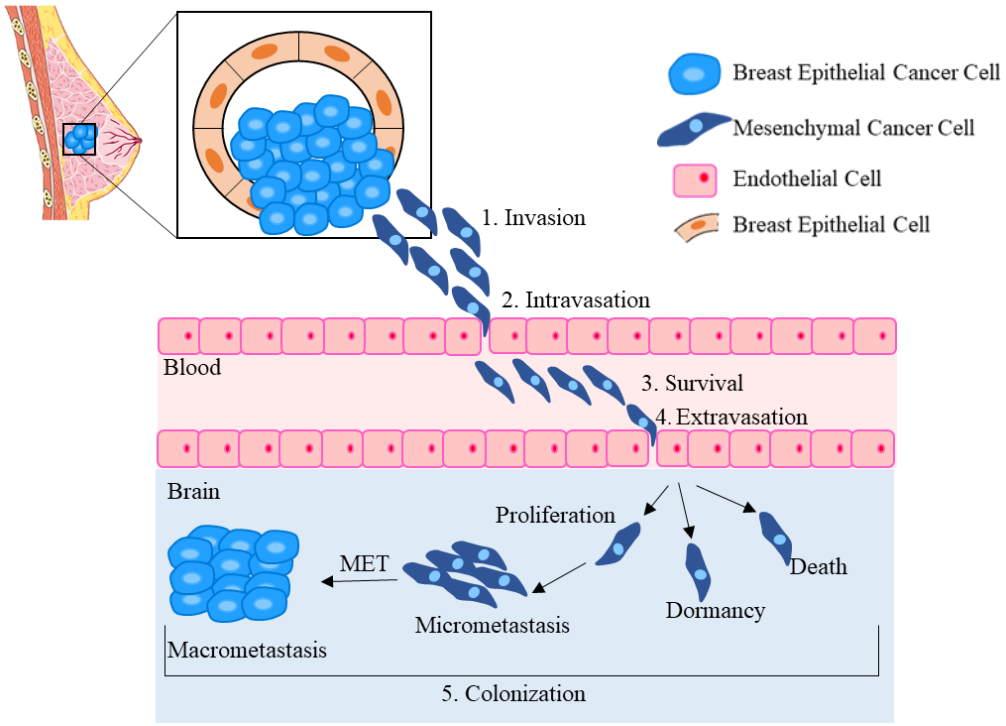

Figure 1.1. Schematic representation of the metastatic process leading to the formation of brain metastases. After the formation of the primary tumor, due to excess proliferation of breast cancer cells (BCCs), these cells have the ability to change their phenotype from epithelial to mesenchymal, a process known as epithelial-mesenchymal transition (EMT), through which they become invasive and migratory, managing to escape from the ducts into the surrounding tissue (1). The next step involves the entry of BCCs into the bloodstream (2), through which they can be transported throughout the body and need to survive inside the blood vessels (3). The most resistant cells move on to the next step, which consists of extravasation to the brain (4). Upon entry, cells can have 3 fates: death, dormancy, and proliferation. Those with greater proliferative capacity form micrometastases, in which the cells undergo mesenchymal-epithelial transition (MET) and lead to the formation of macrometastases, thus completing the last stage of the metastatic cascade, which consists of brain colonization (5).

Studies have shown that the interaction between tumor cells with the brain microenvironment is essential for tumor cell growth and metastasis formation, where BCCs that metastasize to the brain acquire brain

cell properties as a malignant adaptation to promote their survival, proliferation and successful brain parenchyma colonization [15]. In the brain, BCCs can have 3 fates: cell death through apoptosis; dormancy, where they can remain inactive for years or can remain in a proliferative state leading to the formation of BM [5]. Malignant cells that acquire the dormant state present a perivascular location, solitary, or organized into tiny clusters, by establishing a persistent association with the vasculature. Since its strategic location on the abluminal side of the capillaries allows an ideal supply of oxygen and access to nutrients, this connection with brain microvascular endothelial cells (BMECs), allows the BCCs' survival, as well as their successful proliferation and metastases development [5]. The transition to a proliferative state is influenced by the interactions between the tumor cells and the extracellular matrix (ECM), as well as by the drastic reorganization of the cytoskeleton with the activation of the myosin light chain kinase [5, 15, 18]. On the other hand, cells that acquire a proliferative state remain in contact with BMECs and undergo a process named as vascular cooption. Vascular cooption is the mechanism by which the tumor mass acquires oxygen and nutrients, essential for its growth and dissemination in the brain, through pre-existing vessels, independently of angiogenesis occurrence. Even in a micrometastatic state (small cluster of BCCs), malignant cells also establish interactions with brain cells like astrocytes that protect them from chemotherapeutic drug-induced apoptosis, and produce matrix metalloproteinases (MMPs), growth factors and chemokines. Other brain cells such as pericytes, regulate the development, stabilization, and remodeling of preexisting vessels. Besides these interactions, malignant cells also acquire the ability to exploit endogenous brain substrates secreted by neighboring parenchymal cells, allowing them to grow in the brain [5, 15, 18]. The transition from micrometastasis to macrometastasis is characterized by the reacquisition of the epithelial phenotype by the BCCs. These changes in protein expression promote the adaptation, integration, and survival of metastatic cells in the brain. When the tumor mass reaches macroscopic size, angiogenesis is stimulated. [5, 15, 18]. Thus, the most metastatic cells that form robust macrometastases are able to terminate the metastatic process [5].

Combining the high incidence of BM with the low efficacy of therapies applied in BM eradication, the development of new therapeutic strategies is essential and urgent to reduce mortality and increase the quality of life associated with TNBC metastases.

1.2 Platelet-derived growth factor subunit B as an influencer on cancer cell tumorigenesis

The platelet-derived growth factor B subunit (PDGF-B) is a growth factor that is part of the PDGF family and is known for its crucial role in embryological development. PDGF-B dimerizes the cell surface receptors α and β (PDGFRα and PDGFRβ, respectively), originating the phosphorylation of downstream targets by the intracellular receptor kinase domain. These molecular events activate a signaling cascade that promotes the expression of growth factors and their receptors, which is essential for embryonic proliferation and formation of a healthy organism [19-21]. PDGF-B also promotes cytoskeleton remodeling and cell motility [19]. However, recent studies have shown that PDGF-B can act as an oncogene when it is expressed at high levels, which can lead to a variety of neoplasms, in particular brain tumors [19, 22]. Studies developed by our group showed that BM associated with TNBC are associated with an increase of PDGF-B expression [23].

Some studies have demonstrated increased PDGF-B expression in highly invasive glioma cells [24] and human breast carcinoma cells with invasive phenotype [25]. It was also demonstrated that the autocrine PDGF-B signaling contributes to the maintenance of EMT and metastases formation, playing a crucial role during tumor progression [25]. Importantly, PDGF-B has also been identified as an exclusive

prognostic marker for BM in BC patients [26]. Moreover, it was observed that the overexpression of PDGF-B induces DNA damage response, genomic instability, ploidy in glial cells, and hyperplastic lesions of the brain, subsequently leading to replicative stress and ultimately resulting in tumorigenesis [27]. The same study also demonstrated that the use of a PDGF-B inhibitor induces a decrease in the incidence of oncogene-induced glioma, which prolongs survival of this patients, and reduces genomic instability in tumors [27].

PDGF-B is a growth factor also studied for its critical role in vascular remodulation, being described to support the maturity and functionality of blood vessels, which leads to increased angiogenesis [23, 28]. It has been demonstrated that PDGF-B has a dominant expression near to blood vessels, responsible for ensuring an adequate supply of oxygen and nutrients for the proliferation of metastatic cells [23]. All of this leads to tumor aggressiveness, due to increased angiogenesis, tumor invasion, and a higher rate of metastasis formation. In line with this, PDGF-B knockdown was demonstrated to induce vessel normalization, improving its functionality and maturation to suppress angiogenesis, thus, indicating that downregulation of PDGF-B limits the formation of metastases and improves chemosensitization [28].

In line with the studies mentioned above and the fact that PDGF-B appears to be involved in the early and sustained proliferation of BCCs the use of nucleic acid-based strategies that interfere with the expression of the gene encoding this growth factor could be an excellent strategy to combat BCBM.

1.2.1 Nucleic acid-based strategies for brain metastases: Potential and obstacles

The use of nucleic acid-based strategies has been shown to have great potential to generate highly specific and biocompatible drugs [29, 30]. Typically, these strategies are based on gene silencing. Gene silencing usually consists of an epigenetic modification causing the inactivation of the target genes. It can occur at the post-transcriptional level, where there is messenger RNA (mRNA) degradation or translation repression. These effects are usually regulated by small RNAs, such as interfering RNAs (iRNAs) [31]. Small interfering RNA (siRNA) is a class of non-coding double-stranded RNA molecules that act as iRNA [32], which have the ability to bind to a mRNA of a specific gene, such as the gene that encodes PDGF-B, through the complementarity between nucleotides and cause its degradation or block the mRNA so that translation does not occur [33]. Since there is no growth factor synthesis, all functions performed by PDGF-B are compromised. However, the use of these molecules has intrinsic limitations that restrict their *in vivo* administration, such as poor pharmacokinetics, easy degradation by nucleases, rapid blood clearance, low biological stability, and inability to target specific tissues or cells. Even when they are able to reach target cells, their negative charge and hydrophilic nature impair cell internalization [29, 30].

In addition to all the limitations mentioned above, there is still a major obstacle in the application of gene therapies for BM treatment: the existence of the BBB which is a dynamic and complex interface between the blood and the CNS that strictly controls exchanges between the blood and brain compartments [34]. The anatomical basis of BBB is formed by BMECs characterized by the presence of elaborate junctional complexes, such as tight and adherens junctions that act to restrict permeability through the endothelium, as well as gap junctions that mediate intercellular communication [35]. Given these characteristics, the BBB prevents 98% of drugs from passing through and reaching the brain [34]. Considering the potential of using nucleic acid-based strategies, as well as all their limitations, the development of new transport vehicles that are efficient in the delivery of siRNA and that can cross the BBB is essential and urgent for the treatment of TNBC metastases.

1.3 Central nervous system: a big challenge for small interfering RNA delivery

Over the past 30 years, the use of liposomes as convenient delivery vehicles for biologically active compounds has grown, mainly in the field of oncology due to their high biocompatibility, favorable

pharmacokinetic profile and easy surface tailoring [36]. These spherical lipid bilayers can have a wide range of sizes (50-1000 nm), phospholipid composition, and surface characteristics that suit their different applications [37]. Liposomes as nanocarriers have been explored in the health field, from drug delivery to tumor imaging [38]. Nanocarriers have also been widely used in vaccine development, as is the case with vaccines against covid-19 [39]. Due to its high efficiency in drug delivery, its usage in the treatment of cancers for the delivery of chemotherapeutic drugs is a state-of-the-art technology [40].

In order to overcome the disadvantages in the application of siRNA technology for the treatment of cancers, a new class of lipid-based nanosystems has been developed and shown to be very efficient in delivering siRNAs, both *in vitro* and *in vivo* [30]. These particles are called stable nucleic acid lipid particles (SNALPs). SNALPs were first developed in 2001, by Semple and colleagues, and are considered an evolution of cationic liposomes for nucleic acid delivery [41]. Typically, SNALPs have an average size of 100 nm and are composed of an ionizable cationic lipid, a polyethylene glycol (PEG-lipid), and helper lipids. 1,2-Dioleoyl-3-dimethylammonium propane (DODAP) is an ionizable cationic lipid that promotes high siRNA encapsulation [30, 41]. The PEG-derivatized lipid in the liposomal formulation allows for a longer circulation time in the blood, since this type of nanocarriers are not recognized by the reticuloendothelial system [30, 41, 42]. The SNALP formulation fulfills most/all of the requirements for the intravenous administration of siRNA, such as high encapsulation efficiency, small size, electrical neutrality, and high protection against enzymatic degradation [29, 30].

In the last 15 years, the application of these lipid particles has been shown to be effective in the delivery of siRNAs for the treatment of several pathologies [43-47] . Morrissey and colleagues demonstrated the specific silencing effect of siRNAs formulated with SNALPs targeting the hepatitis B virus in an *in vivo* mouse model [46]. Shortly after, Zimmermann and colleagues demonstrated the efficacy of siRNA encapsulation against apolipoprotein B in non-rodent species (cynomolgus monkeys) [47]. The effectiveness of SNALPs against Ebola virus has also been studied by Geisbert's team, who have shown that iRNA-based therapy can hold promise for treating people infected not only with the Ebola virus, but also with other viral infections [45]. Currently, the only commercially available drug based on SNALP technology is patisiran (ONPATTRO^{TM}) [as review in [44]]. This drug is a therapeutic agent based on iRNA technology that specifically inhibits hepatic transthyretin synthesis and is used in patients with Transthyretin Amyloidosis. The use of this drug reduces the amount of transthyretin, which leads to a reduction in pathological manifestations of the disease, as well as an improvement in the quality of life of patients [43].

Particularly in oncology, the use of SNALPs was demonstrated by Judge and colleagues, which developed a siRNA delivery system targeting essential cell cycle proteins: polo-like kinase 1 and spindle protein kinesin, and found a potent antitumor effect in liver and subcutaneous tumor models, as well as a minimization of non-specific effects [48]. Furthermore, the effectiveness of siRNA directed to a microRNA for the treatment of multiple myeloma was also studied and demonstrated that the use of SNALPs was highly efficient in inhibiting the growth of tumor cells, translating into an increase in the survival of the studied mice [49]. Several studies were also carried out to study the relevance of SNALPs in the treatment of neurological pathologies, Pedroso de Lima and colleagues have demonstrated the efficacy of using lipid particles to target mutant ataxin-3 gene for the treatment of patients with Machado-Joseph disease [50]. Another group of scientists has demonstrated the effectiveness of siRNA encapsulation in SNALPs against glioma cells [29]. These last two examples are only possible, since SNALPs have the ability to cross the BBB and it is important to highlight that SNALPs can be designed to allow either (1) receptor-mediated or (2) absorption-mediated transcytosis [51], as depicted in **Figure 1.2**. Transcytosis is a type of transcellular transport of molecules through vesicles, in which the macromolecules are endocytosed or internalized in vesicles on one side of the cell and transported to the other side where they are released or exocytosed [52]. Absorption-mediated transcytosis is characterized by interactions between molecules and the cell membrane that facilitates the transport across the barrier

[52]. In the case of SNALPs, size and surface charge are essential features for lipid particles to cross BBB [51]. On the other hand, receptor-mediated transcytosis occurs due to the use of ligands that bind to receptors expressed on the BBB endothelium surface [51, 52]. Many ligands have already been shown to be effective and safe in overcoming the BBB, such as chlorotoxin (CTX) [51].

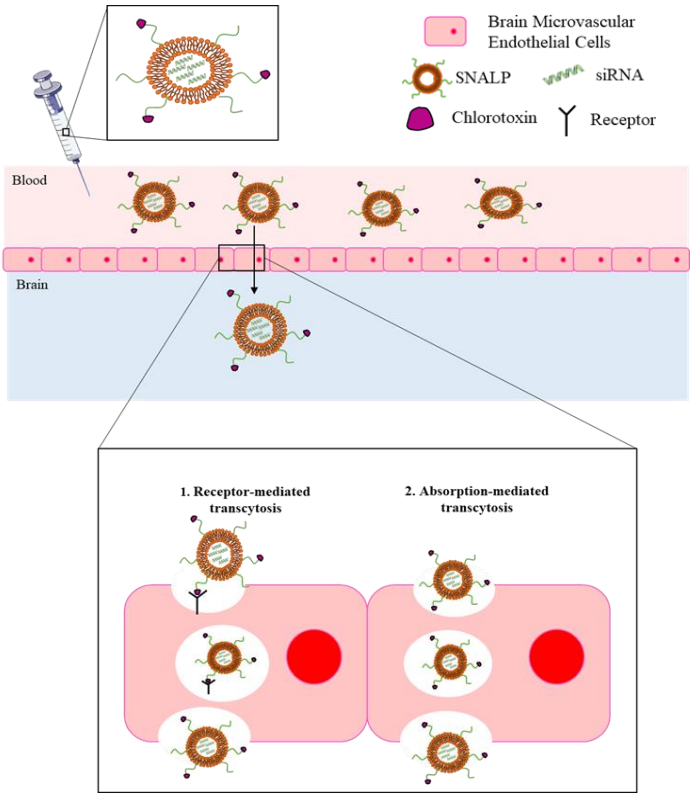

Figure 1.2. Schematic representation of a proposed mechanism of the passage of SNALPs through blood-brain barrier. Lipid particles that carry siRNA are injected intravenously and transported by the blood. Upon reaching the BBB, which is formed by a monolayer of endothelial cells, liposomes need to process characteristic to effectively enter in the brain. SNALPs have two different mechanisms to cross the BBB: (1) receptor-mediated transcytosis, where the nanocarrier ligand binds to the receptor present in the plasma membrane allowing the formation of a vesicle around the complex that facilitates its endocytosis into the brain; or (2) absorption-mediated transcytosis, which consists in the formation of endocytosis vesicles through the interaction between the membrane and the lipid particle without the involvement of receptors. In this last mechanism the charge and size of SNALPs are essential for passage through the BBB.

1.3.1 Chlorotoxin as a target ligand

As mentioned above, one of the main problems in the application of therapies is passing through the BBB, thus some studies have shown that CTX is able to cross the BBB without causing its damage [53, 54] and can act as a targeting ligand. CTX is a peptide with 36 amino acids and 4 disulfide bonds, originally isolated from the venom of the *Leiurus quinquestriatus* scorpion. Although the specific receptors to which CTX binds to successfully bypass the BBB remains unclear [51], the use of CTX on the surface of nanocarriers revealed an accumulation of nanocarriers in the brain tumor, as in glioblastoma, and also allowed the delivery of siRNA to the brain after systemic injection [55]. These indicate that CTX can facilitate the crossover of liposomes through the BBB.

The peptide CTX was shown to have a high affinity for cancer cells, selectively binding to glioma cells and other tumors of neuroectodermal origin, without binding to resident brain cells. In this way, it can act as a marker of brain tumors, due to its selective binding properties [53, 56-58]. Early studies have shown that CTX blocks chloride-channels in glioma cells, which inhibits tumor cell migration [59]. It has also been demonstrated that CTX has the property of binding to MMP-2, which is an up-regulated receptor in tumor cells from gliomas and related cancers, although it is poorly expressed in the brain and normal tissues [56, 60]. Moreover, other studies demonstrated that direct binding of CTX to MMP-

2 decreases gelatinase activity, reducing the cell invasion ability. This interaction has also been shown to cause a decrease of MMP-2 expression due to its cellular internalization via caveolae mediated endocytosis of the complex. This fact suggests that CTX, through modulation of MMP-2 expression on the cell surface, regulates the invasive potential of tumor cells. Thus, the CTX is an important component with relevant therapeutic implications in the treatment of invasive gliomas [60].

Taking in account the characteristics of MMP-2, the use of CTX coupled to SNALPs may be of advantage for targeting tumor cells. Costa et al. studied SNALPs copulated with CTX and demonstrated an increased association and internalization in glioma cells, while in normal cells there is a decrease in its affinity. These authors also showed an increase in the delivery of siRNAs, thus reducing the toxicity associated with their systemic administration and causing a greater effect in the treatment [29]. Moreover, the CTX-modified delivery system was described effective in BCBM, due to the overexpression of MMP-2 in BCCs [56, 61]. Qin and colleagues have demonstrated that the development of a CTX-coupled liposome increases its uptake and toxicity in BCCs, liposome targeting *in vivo*, antitumor and antimetastatic efficacy, and still decreases systemic toxicity [56]. These studies demonstrate that the use of CTX-coupled SNALPs has adequate physicochemical properties for siRNA delivery, intravenous administration, crossing the BBB, and targeting BCCs.

Despite all the evidence that the use of CTX coupled to nanocarriers may improve siRNA delivery and help in crossing the BBB, further studies are needed to examine the influence of these lipid particles in the treatment of BCBM.

1.4 Salinomycin as a potential new drug for brain metastasis treatment

The main obstacle in treatment of cancer is the acquisition of resistance by tumor cells to the different existing drugs. So, the discovery of new drugs that are effective in the fight against cancer progression is essential. The main mechanisms by which cells acquire resistance are reduced absorption of water-soluble drugs; variety of cell changes, such as increased DNA repair, cell cycle protein changes; and reduced level of apoptosis and hydrophobic drug efflux via (ATP-binding cassette) ABC transporter. This last mechanism plays a vital role in making BCCs multidrug resistant. Therefore, compounds with tumor proliferation inhibitory properties, such as salinomycin (SAL), have been studied with the aim of helping to overcome the obstacle of drug resistance [62].

SAL is a hydrophobic monocarboxylic polyester antibiotic derived from *Streptomyces albus*. It has a high affinity for positive ions, with a preference for potassium, acting as a membrane ionophore. Studies have shown that SAL selectively kills BC stem cells much more effectively than drugs commonly used in chemotherapy and inhibits breast tumor growth in mice [62, 63]. This drug mediates its cancer effect through several mechanisms in different types of cancer. It has the ability to reduce the activity of ABC transporters in leukemia stem cells, inhibit the Wnt signaling cascade in colorectal cancer cells [64], as well as the cell growth and migration of prostate cancer [65], also leading to accumulation of reactive oxygen species in prostate cancers [66]. Moreover, it induces apoptosis in human hepatocellular carcinoma cells [67], and autophagic response in prostate cells and BCCs [68]. SAL has been shown to have a cytotoxic effect due to disruption of the balance of sodium and potassium ions at the cell membrane and mitochondria, which causes cell apoptosis [64, 69]. Lower expression of epithelial (E)-cadherin makes cells more resistant to drugs and promotes transition EMT, however, it has also been shown that SAL is able to eliminate cells that express reduced amounts of E-cadherin [70].

Several studies have focused on the effect of SAL on human and mouse TNBC cells (MDA-MB-231 and 4T1, respectively). It was observed that SAL causes downregulation of signal transducer and activator of transcription 3 (STAT3) leading to an inhibition of cancer stem cells (CSCs) [71], since STAT3 is involved in cell proliferation and survival. It reduces the expression of cyclin D1 leading to cell death [72] and also causes an increase in histone acetylation's which leads to an increase in cell

death and senescence [73]. Another study also showed that SAL causes anoikis in tumor cells, which is a specific form of cell death by cell detachment from the ECM, and activation of caspases. Finally, SAL has also been shown to be toxic to TNBC cells [71], whereas non-tumor cells were able to avoid the toxic effect [74]. Another study showed that 4T1 cell metastasis upon SAL treatment exhibited a 4-fold reduction in metastasis formation compared to untreated cells [75]. Moreover, 4T1 cells treated with SAL have an epithelial-like morphology, with higher expression of E-cadherin (epithelial marker) and lower expression of vimentin (mesenchymal marker). It also showed that treatment with this cytotoxic agent leads to the loss of genes associated with CSC, generally correlated with poor prognosis tumors, that is, there is a significant reduction in the expression of genes that promote invasiveness and differentiation [75]. Finally, exposure to SAL significantly decreases the mRNA abundance of MMP-9 and MMP-2, which causes a decrease in cell migration and invasion [71]. Therefore, SAL has the potential to be applied as a new drug for the treatment of TNBC.

Regardless of all the chemotherapeutic effects of SAL, it is known that in humans it causes secondary symptoms such as shortness of breath, dizziness, nausea, leg weakness, photophobia, and increased blood pressure [62]. To add to these symptoms, its hydrophobic property leads to a low activation at the active site, consequently a low bioavailability [36]. Thus, the development and use of lipid particles for the transport of this drug, can be essential to reduce toxicity, reduce the side effects associated with the use of the drug, prolong drug circulation time, increase tumor targeting, and potentiate SAL's therapeutic effect.

1.4.1 Liposomes as a salinomycin delivery system

The use of liposomes to deliver SAL has been shown to be efficient by improving therapeutic effects, while decreasing side effects to other tissues. Several types of SAL-containing liposomes were studied, most of which contained PEG on the surface to prolong circulation time concentration of the drug in the blood [36]. Kim et al. studied the efficiency of using a liposome encapsulating SAL and doxorubicin (Dox) against BCCs, having demonstrated that the use of a dual liposome could increase the cytotoxic potential against BC, controlling the pharmacokinetics and distribution *in vivo* [76]. Gong et al. studied the same drugs against liver cancer cells, having shown an inhibition of the tumor and a decrease of CSCs. Liposomes still exhibited prolonged half-life and decreased clearance *in vivo* [77]. Xie et al. developed liposomes with SAL and chloroquine and demonstrated their cytotoxic effect on liver cancer cells [78]. Momekova et al. encapsulated SAL derivatives and studied their effect on different cell lines, demonstrating that incorporation into liposomes could lead to superior effects of the free form of the drug [79].

The dehydration–rehydration method (DRV) was developed in 1984 by Gregoriadis and colleagues, is one of the most commonly used methods for the preparation of liposomes [80]. It is characterized by encapsulate a wide variety of materials into liposomes of variable lipid compositions, with high efficiency and using mild conditions [80]. So, in short, the development of a coadministration strategy, which combines pharmacological and genetic therapy both associated with liposome nanotechnology, as shown in **Figure 1.3**, appears an excellent strategy. Liposomes are used as delivery systems to increase the anticancer effects of both drugs, while reducing potential side effects. In this way, coadministration allows for synchronized delivery.

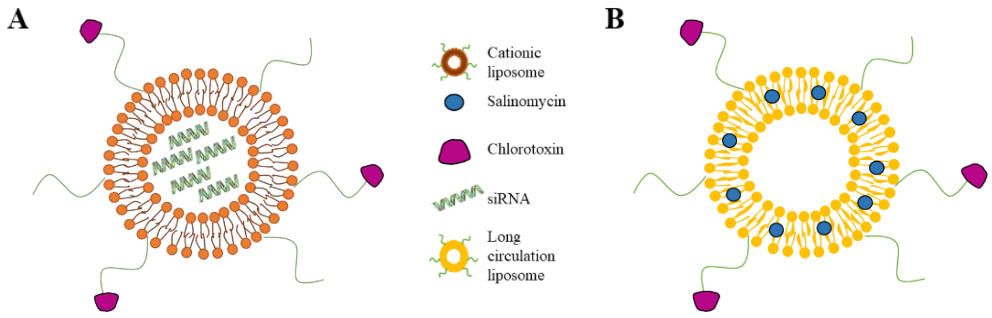

Figure 1.3 Schematic representation of two different lipid particles that encapsulate a siRNA and a drug. (**A**) SNALPs (average size of 100 nm) composed of an ionizable cationic lipid, a polyethylene glycol (PEG-lipid) and lipid helpers. These lipid particles are efficient nanocarriers for intravenous administration of siRNA. (**B**) Liposomes (average size of 120 nm) composed of Egg Phosphatidylcholine and a PEG-lipid on surface. These lipid particles are efficient in delivering salinomycin. These nanocarriers can become more specific through the insertion of small peptides, such as chlorotoxin, which target breast cancer cells.

II. Aim

The lack of treatment options that efficiently cross the BBB, and are effective against BCBM led to this project. The main objective was the development of a new therapeutic approach for BCBM eradication. Therefore, this work will test the hypothesis that the use a new platform of nanomedecines decorated with CTX for a therapeutic approach that combines a drug (SAL), and genetics (siPDGF-B) could reduce or eradicate BM associated with TNBC. The nanoformulations (NFs) decorated with CTX and encapsulating siPDGF-B (CTX-siPDGF-B-SNALPs) were already developed and characterized (Joana Godinho-Pereira, PhD thesis, Faculdade de Farmácia, Universidade de Lisboa, ongoing). The work in this tesis consists of the efficient SAL incorporation, as well as performing cellular studies to evaluate the effectiveness of a siPDGF-B and SAL for the eradication of TNBC in a BBB-BCCs co-culture system. To achieve the main objective, specific tasks were outlined:

1. Evaluate the ability of the CTX-siPDGF-B-SNALPs to decrease BCCs viability and verify the inhibitory action of the encapsulated siRNA on PDGF-B expression;
2. Study the incorporation efficiency of Sal in a liposome;
3. Evaluate the ability of the incorporated SAL to harm the viability of BCCs and determinate its median lethal dose (LD50);
4. Evaluate the ability of the combined approach to decrease BCCs viability, modulate proliferative properties of BCCs and verify their inhibitory action on PDGF-B expression;
5. Ensure the NFs safety for the BBB endothelium;
6. Evaluate the effectiveness of the combined approach in BBB permeation and action on malignant cells in a simplified *in vitro* model of BCBM by evaluation of PDGF-B expression and senescence.

With this study, we intend to establish the efficiency of combined approach NFs to eradicate BCCs in an in vitro model of BCBM, as well as its tolerability by host cells. This work will open new paths for a new treatment for patients with BM associated with TNBC. Thus, the success of this investigation work shall contribute to a great advance in the field of Neurooncology, as well as to an improvement in the expectation and quality of life of TNBC patients.

III. Material and methods

3.1 Cell Culture Conditions and Treatment

3.1.1 Breast cancer cells

The 4T1 triple negative murine mammary carcinoma cell line (ATCC, Middlesex, UK) was used. These cells were cultured in Roswell Park Memorial Institute (RPMI) medium 1640 (Sigma Aldrich, St. Louis, MO, USA) supplemented with 5% (v/v) fetal bovine serum (FBS, Biochrom AG, Berlin, Germany), 1% antibiotic-antimycotic solution (Sigma Aldrich) and 2 mM L-glutamine (Biochrom AG). Cells were maintained at 37°C in a humid atmosphere enriched with 5% CO_2.

3.1.2 Endothelial cells

The mouse brain microvascular endothelial cell line b.End5 (ECACC, Salisbury, UK) was used. b.End5 cells were maintained in Dulbecco's modified Eagle's medium (DMEM, Gibco, Life Technologies, New York, NY, USA) supplemented with 10% FBS (Biochrom AG), 1% non-essential amino acids (Biochrom AG), 2 mM L-glutamine (Biochrom AG), 1 mM sodium pyruvate (Biochrom AG) and 1% antibiotic-antimycotic solution (Biochrom AG) at 37 °C in humid atmosphere enriched with 5% CO_2.

3.1.3 Co-culture

Co-cultures of b.End5 cells and 4T1 cells were used as a simplified *in vitro* model of BCBM. In this model, endothelial cells were plated onto semi-permeable membranes (Transwell inserts, VWR International, Radnor, PA, USA) with the luminal surface facing the upper compartment ("blood" side) and BCCs were plated on the bottom of the cell culture plate ("brain" side). 80000 b.End5 cells seeded onto Transwell inserts (0.4 μm pore) were grown for 3 days until a monolayer was formed, and then 500 nM hydrocortisone was added to improve BBB features. On day 4, $1x10^5$ cells/mL of 4T1 cells were seeded onto 12-well plates and let grow for 24 h. Then, the inserts were placed on the well with 4T1 cells and the co-cultures proceeded for 1 h, and liposomes were administered in the upper ("blood") compartment.

3.1.4 Cell treatment

Cells in single and co-cultures were treated with the developed formulations (described below). 4T1 cells viability, PDGF-B expression and proliferative properties were determined by the resazurin assay, RT-qPCR and immunofluorescence analysis, respectively, to establish the efficacy of the NFs. b.End5 cells were assessed for the viability (resazurin), transendotelial electrical resistance (TEER) and β-catenin expression (immunofluorescence) to detect any potential toxicity of the NFs. Finally, co-cultures were used to ascertain the efficacy of the BBB-permeant fraction of the NFs in modulating the expression of PDGF-B and p16 in 4T1 cells, as well as to monitor the endothelial integrity.

3.2 Lipid nanoformulations preparation

3.2.1 siRNA-encapsulated liposomal formulation

siRNA formulation was implemented in our laboratory by Joana Godinho-Pereira (PhD thesis, Faculdade de Farmácia, Universidade de Lisboa, ongoing) based on previous publications [29, 30, 81]. Briefly, liposomes composed by DODAP, distearoylphosphatidylcholine (DSPC), cholesterol (Chol), and N-palmitoyl-sphingosine-1-[succinyl(methoxypolyethylene glycol) 2000] (CerC16-PEG200) (Avanti Polar Lipids, Alabama, USA) in a molar ratio of DODAP:DSPC:Chol:CerC16-PEG2000 at 25:22:45:8 were prepared by ethanol injection method together with 41 nmol of siRNA (siScramble or siPDGF-B) in 500 μL of total volume. Thirteen micromoles of the lipid mixture were dissolved in 200 μL of absolute ethanol and then heated to 60°C. The lipid mixture was added dropwise, under strong vortex, to the siRNA in 300 μL of citrate buffer (20 mM, pH 4.0), previously warmed at 60ºC. The resulting multilamellar particles were extruded 21 times through 100 nm diameter polycarbonate membranes using a Mini-Extruder SET (Avanti Polar Lipids). The exchange of ethanol for citrate buffer was done through a 2 h dialysis against citrate buffer, followed by overnight dialysis against HEPES

buffer (20 mM HEPES, 145 mM NaCl, pH 7.4) in order to exchange the citrate buffer for the HEPES buffer.

3.2.2 Salinomycin and siRNA-encapsulated liposomal formulation

In the co-encapsulation of SAL and siRNA, liposomes composed by DODAP:DSPC:Chol:CerC16-PEG2000 were prepared by the ethanol injection method in a different molar ratios in order to identify the best one, as show in **Table 3-1**.

Table 3-1 Molar ratio test at SAL incorporation in SNALP

Formulation	Lipid composition	Lipid concentration (µmol/ml)
A	DODAP:DSPC:Chol: CerC16-PEG200 (25:22:45:8)	26
B	DODAP:DSPC:Chol: CerC16-PEG200 (25:45:22:8)	26
C	DODAP:DSPC:Chol:CerC16-PEG200 (25:45:22:8) (WITH siRNA)	26

Chol: cholesterol, CERC16-PEG200: N-palmitoyl-sphingosine-1-[succinyl(methoxypolyethylene glycol) 2000]; DODAP:1,2-dioleoyl-3-dimethylammonium propane, DSPC: distearoylphosphatidylcholine

Briefly, SAL was dissolved together with thirteen micromoles of the lipid mixture and the rest of the preparation was carried out as describe in section 3.2.1. For formulation A and B, as we wanted to just test the efficacy of SAL incorporation into the liposome, SNALPs did not had neither siRNA nor CTX. In the formulation C siRNA was added in the citrate.

3.2.3 Salinomycin-encapsulated liposomal formulation

In order to study which liposomes had the highest SAL incorporation efficiency, liposomes composed by different lipid mixture and molar ratio were prepared, as described in **Table 3-2**.

Table 3-2 Lipid mixture and molar ratio test at SAL incorporation in a liposome

Formulation	Lipid composition	Lipid concentration (µmol/ml)
D	DSPC:Chol:DSPE-PEG (85:10:5)	13
E	EPC:Chol: DSPE-PEG (85:10:5)	13
F	EPC:Chol: DSPE-PEG (85:10:5)	26
G	DSPC:Chol: DSPE-PEG (85:10:5)	26
H	DOPE:CHEMS:DMPC: DSPE-PEG (37.5:20:37.5:5)	26
I	DPPC:DPPG: DSPE-PEG (85:10:5)	26
J	DMPC:DMPG: DSPE-PEG (85:10:5)	26
K	DOPC:DOPG: DSPE-PEG (85:10:5)	26
L	DSPC: DSPE-PEG (95:5)	26
M	EPC: DSPE-PEG (95:5)	26

Chol: cholesterol, CHEMS: cholesteryl hemisuccinate, DSPC: distearoylphosphatidylcholine, DSPE-PEG: distearoyl-glycerophosphorylethanolamine–poly(ethyleneglycol)2000, DMPC: 1,2-dimyristoyl-sn-glycero-3-phosphocholine, DMPG: 1,2-dimyristoyl-sn-glycero-3-phosphoglycerol, DOPC: 1,2-dioleoyl-sn-glycero-3-phosphocholine, DOPE: 1,2-dioleoyl-sn-glycero-3-phosphoethanolamine, DOPG: 1,2-dioleoyl-sn-glycero-3-[phospho-rac-(1-glycerol)], DPPC: 1,2-dipalmitoyl-sn-glycero-3-phosphocholine, DPPG: 1,2-Dipalmitoyl-sn-glycero-3-phosphoglycerol, EPC: egg phosphatidylcholine,

Liposomes were prepared by the thin film method. Briefly, the lipid mixture and SAL were dissolved in chloroform. A thin film of lipids and drug film was obtained by evaporation under vacuum in a rotary evaporator (Buchi R-200, Flawil, Switzerland). The thin film was stored in -20ºC. In the next day, the film was hydrated with HEPES buffer, under vortex. This step was followed by extrusion in an extruder device (LipexBiomembranes, Vancouver, Canada) to down-size the liposomes by sequential extrusion through polycarbonate filters ranging from 0.8 to 0.1 μm in pore size. To separate the non-entrapped SAL, size exclusion chromatography using a desalting column with a 1000 Dalton cutoff was used (Econo-Pac®, BIO-RAD, Hercules, CA, USA).

3.2.4 Salinomycin-encapsulated liposomal formulation optimization

Once the liposomal formulation with the highest encapsulated SAL efficiency was determined, the process was optimized. Briefly, liposomes composed by egg phosphatidylcholine (EPC) and distearoyl-glycerophosphorylethanolamine–poly(ethyleneglycol)2000 (DSPE-PEG) (Avanti Polar Lipids) were prepared by DRV method in a molar ratio of EPC:DSPE-PEG at 95:5 together with 5 μmol/mL of SAL. 26 μmol/mL of the lipid mixture and 5 μmol/mL SAL were dissolved in chloroform. A thin lipid and drug film was obtained by evaporation under vacuum in a rotary evaporator (Buchi R-200). The thin film was hydrated with water and freeze-dried overnight (EDWARDS, Modulyo, CO, USA). Thereafter, the lyophilized powder was hydrated with HEPES buffer, under vortex and the solution was extruded, as described in section 3.2.3. From this point on, the preparation took place as described in previous section.

3.2.5 Chlorotoxin conjugation to nanoformulations

Targeted liposomes were prepared by the postinsertion method, as described in [29]. Briefly, a film lipid of 1,2-distearoyl-sn-glycero-3-phospatidylethanolamine-N-[maleimide (polyethylene glycol)-2000] ammonium salt (DSPE-PEG-MAL) (Avanti Polar Lipid) was formed by evaporating the solvent under a nitrogen flux. The film was kept at -20ºC until micelles formation. CTX was activated by the addition of thiol groups through reaction with freshly prepared 2-iminothiolane hydrochloride (2-IT) in HEPES-buffer 8.0 (20 mM HEPES, 145 mM NaCl, pH 8.0) at a molar ratio of 1:10 (CTX:2-IT), during 1 hour in the dark at room temperature (RT) under gentle stirring. Micelles were formed by hydration with MES buffer (20 mM HEPES, 20 mM MES, 145 mM NaCl pH 6.5) under two cycles of strong vortex and heating at 37ºC. Then, thiolated CTX was coupled to micelles (1:5, CTX:DSPE-PEG-MAL molar ratio) via a thioesther linkage overnight at RT in the dark with gentle stirring. Next, free maleimide groups were neutralized with β-mercaptoethanol (1:5 molar ratio), under stirring for 30 min at RT. The insertion of CTX:DSPE-PEG-MAL conjugates into the preformed liposomes, at 4 mol % for the SNALPs or 2 mol% for the SAL liposomes was performed upon incubation in a water bath at 39ºC overnight for the SNALPs and RT for the SAL formulation, both in the dark. The last step consists of removing all external chemical reagents used during liposomal preparation. Sepharose CL-4B column equilibrated with HEPES buffer was used in the CTX-siPDGF-B-SNALPs whereas ultracentrifugation (Beckman LM-80 ultracentrifuge) was performed in the liposomes decorated with CTX incorporating SAL (CTX-SAL-Lip). The pellet was then resuspended in HEPES buffer.

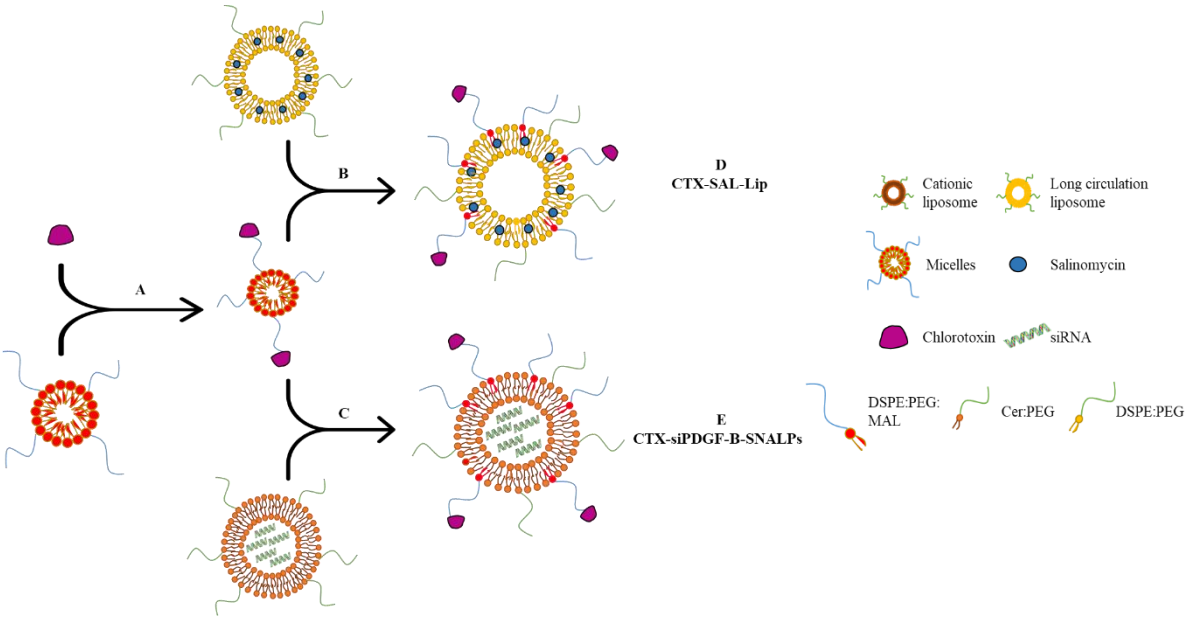

Figure 3.1 Schematic representation of pos-insertion method. (**A**) After CTX activation, the peptide is incubated with the micelles in order to bind on the surface. The targeted micelles are incubated with previously prepared (**B**) SAL-Lip or (**C**) siPDGF-B-SNALPs. The micelles incorporate the surface of the liposomes (represented by the red lipids) forming the final liposome (**D**) CTX-SAL-Lip or (**E**) CTX-siPDGF-B-SNALPs.

3.2.6 Liposomal characterization

To characterize the developed liposomal formulations, the physicochemical parameters were determined, as well as the Chol/phospholipid, CTX, and SAL/siRNA contents. The hydrodynamic diameter (z-average) and polydispersity index (PDI), which serve as a measure of homogeneity, were measured in Zetasizer Nano S (Malvern). For these measurements, liposomes were diluted 1:1000 in HEPES buffer.

The Chol or the phospholipid content of the liposomal formulation were determined by the Liebermann-Buchard method [82] and the phosphate method [83], respectively. For the Chol content, the Liebermann-Burchard reagent [acetic anhydride; acetic acid glacial; sulfuric acid 55:35:10 (v/v)] was added to the sample and incubated at 37°C for 30 min. Afterward, the absorbance of the solutions was measured at 625 nm in a spectrophotometer and the concentration was determined from a standard curve for Chol content. In the colorimetric determination method, for the phospholipid content, the sample were diluted 1:10 in HEPES buffer, and 70% perchloric acid is added to the sample to convert organic phosphate to inorganic phosphorous by hydrolysis at 180ºC. Then, water, 1.25% ammonium molybdate, and 5% ascorbic acid were added to promote the formation of a blue colored compound at 100ºC. The sample was quantified by spectrophotometry at 797 nm and the concentration was determined from a standard curve.

The amount of SAL that was encapsulated was determined by liquid chromatography coupled to a mass spectrophotometer (UHPLC-MS/MS), through a collaboration with investigators of Structural Analysis lab at the Faculty of Pharmacy, an example report is in supplementary material.

The incorporation efficiency (IE %) and the loading capacity (LC µg/µmol) were determined. The IE consists of the percentage of the coefficient between the final SAL-to-lipid ratio ($[SAL/Lip]_f$) and the initial SAL-to-lipid ratio ($[SAL/Lip]_i$). The IE was calculated according to equation 1. The LC is defined as the ratio between the amount of incorporated SAL and the amount of lipid in the final preparation. The LC was determined according to equation 2.

$$\text{IE (\%)} = \frac{[\text{SAL}]_f / [\text{Lip}]_f}{[\text{SAL}]_i / [\text{Lip}]_i} \times 100 \quad (1) \qquad \text{LC (μg/μmol)} = \frac{[\text{SAL}]_f}{[\text{Lip}]_f} \quad (2)$$

The amount of CTX inserted on the surface of SNALPs or SAL liposomes was determined using Bicinchoninic acid (BCA) Protein Assay Kit (Thermo Scientific Pierce, Waltham, MA, USA) from a bovine serum albumin (BSA) standard curve (at 562 nm) in a microplate reader (Biotek, Winooski, Vermont, EUA). The insertion capacity (IC) is defined as the ratio between the amount of inserted CTX and the amount of lipid in the final preparation. The IC was determined according to equation 3.

$$\text{IC (nmol/μmol)} = \frac{[\text{CTX}]_f}{[\text{Lip}]_f} \quad (3)$$

The amount of siRNA encapsulated was also determined in the nanodrop (Eppendorf, Hamburg, Germany). For that, liposomes were incubated with methanol for 3-4 h at a ratio of 1:5, then RNA free water was added at a ratio of 1:2 to the total volume, and reading was performed. For determination was used as blank empty liposomes.

3.3 Cell viability assay

CTX-siPDGF-B-SNALPs and CTX-SAL-Lip toxicity to 4T1 as well as safety for b.End5 cells were evaluated using the resazurin assay, which is based on the reduction of resazurin (blue) to resorufin (pink) in viable cells. Briefly, 4T1 cells were seeded onto a 96 well plate or 24 well plate at a density of 2 x 10^4 cells/mL or 1 x 10^5 cells/mL, respectively. b.End5 cells were seeded onto a 96 well plate at a density of 2.5 x 10^4 cell/mL. At confluence, cells were incubated with different liposome concentrations in DMEM supplemented with 1% antibiotic-antimycotic solution. After 24 h of incubation, medium was discarded and DMEM containing 0.01 mg/mL of resazurin was added to each well. The cells were incubated for 3 h at 37°C. Absorbances values were obtained using a microplate reader (Varioskan LUX Multimode Microplate Reader, Thermo Fisher Scientific, Waltham, MA, USA) at 570 nm and 600 nm, and cell viability was calculated as equation 5.

$$[(A_{570} - A_{600})_{\text{treated cells}} * 100) / (A_{570} - A_{600})_{\text{control cells}}] \quad (5)$$

3.4 Immunofluorescence

The effect of CTX-siPDGF-B-SNALPs and CTX-SAL-Lip on the proliferative properties of 4T1 cells and on b.End5 barrier integrity were studied by immunofluorescence analysis [84] of Ki-67 and of the adherens junction protein β-catenin, respectively. In this assay, 1x10^5 cells/mL of 4T1 and 5 x10^4 cell/mL of b.End5 were plated on coverslips placed in 24-well plates. At the confluence, the medium was removed, and cells were incubated with the liposomes. After 24 h incubation, the cells were fixed with 4% (v/v) paraformaldehyde (PFA, Sigma Aldrich) for 20 min at RT. Following fixation, cells were permeabilized for 5 min with 0.3% Triton-X (VWR International, Radnor, PA, USA) and blocked with 3% BSA (Sigma Aldrich) in phosphate-buffered saline (PBS), for 1 h. Later, cells were incubated with the primary antibody overnight at 4ºC. On the next day, the cells were incubated for 1 h with the secondary antibody at RT. Both primary and secondary antibodies (**Table 3-3**) were diluted in BSA. To stain the nuclei, the cells were further incubated with Hoechst 33342 dye (20 μM, Thermo Fisher Scientific), for 10 min at RT. Between each step, the cells were washed three times with PBS. Finally, the cells were dehydrated in methanol (Honeywell, Charlotte, North Carolina, USA) and mounted in microscopy slides with dibutylphthalate polystyrene xylene (DPX, Merck Millipore, Burlington, MA, USA). Images were acquired using a 40x objective with immersion oil in an Olympus BX60 microscope

equipped with an Olympus U-RFL-T Mercury lamp and Hamamatsu Orca R2 cooed monochromatic CCD camera, at the Microscopy Facility of the Faculty of Sciences of the University of Lisbon.

Table 3-3 Antibodies used for immunofluorescence analysis

Target Protein	Primary antibody	Secondary antibody
Ki-67 (Proliferation marker)	Ki-67 (1:100) Rabbit Thermo Fisher Scientific #PA519462	Alexa Fluor 555 (1:500) Goat anti-rabbit Thermo Fisher Scientific #A21428
β-catenin (Integrity marker)	Beta-catenin (1:100) Rabbit Invitrogen #712700	

3.5 RT-qPCR

The effects of CTX-siPDGF-B-SNALPs and CTX-SAL-Lip on PDGF-B silencing and cell senescence of 4T1 cells were evaluated by RT-qPCR analysis, as usually in our lab [35]. In this experiment, $1x10^5$ cells/mL were plated on a 24 well plate or 12 well plate and after 24 h were incubated with different liposome conditions in DMEM. Following 24 h, the cells were incubated 5 min with trizol to stake cells. The RNA purification was made by chloroform and isopropanol precipitation. Briefly, samples were centrifuged, and chloroform was added to the supernatant. After other centrifugation, the aqueous phase was carefully collected, and isopropanol was added. Next, the resulting pellet was washed in ethanol. Finally, the solution was centrifugated one last time and the pellet was resuspended in diethyl pyrocarbonate (DEPC) water.

RNA was quantified by nanodrop (Eppendorf) and then transcribed into cDNA, using the Xpert cDNA Syntesis SuperMix (Grisp, Porto, Portugal), according to the manufacturer's instructions. The reaction was carried out in a thermocycler (Cleaver, Scientific, UK), under the following conditions: 15 min at 37ºC; 10 min at 60°C; 3 min at 95°C; followed by cooling down and storage at 4°C to stop the reaction. Finally, the RT-qPCR reaction was performed using the Xpert Fast SYBR Green kit (Grisp) according to the manufacturer's instructions using cDNA diluted at 1:2. The reaction was read in QuantStudio™ 7 Flex Real-Time PCR System (Applied Biosystems, Thermo Fisher Scientific). Briefly, the conditions used were 1 cycle of 95°C for 2-3 min, 40 cycles of 95°C for 5 sec, 60-65°C for 20-30 sec, followed by a dissociation/melting curve analysis. Primer pairs (forward and reverse) for PDGF-B, p16 and for the housekeeping gene glyceraldehyde 3-phosphate dehydrogenase (GAPDH) were provided by StabVida (Caparica, Portugal) (sequence in **Table 3-4**). RT-qPCR was performed in 394-well plates, with each condition performed in triplicate, and a no-template control was included for each amplification. The threshold cycle determination was performed using the QuantStudio™ Real-Time PCR software (Applied Biosystems, Thermo Fisher Scientific, Waltham, MA, USA), and the quantifications performed by the ΔΔCt method.

Table 3-4 Resume table of primers sequence for real time quantitative PCR

Target	Primer Sequence	Length (bp)
GAPDH	Forward: 5´-GTG GCA AAG TGG AGA TTG TTG CC -3`	23
	Reverse: 5´- GAT GAT GAC CCG TTT GGC TCC -3`	21
PDGF-B	Forward: `5´- ATC GCC GAG TGC AAG ACG GC -3`	20
	Reverse: 5´- AAG CAC CAT TGG CCG TCC GA -3	20
P16	Forward: 5´- AAC TCT TTC GGT CGT ACC CC -3`	20
	Reverse: 5´- GCG TGC TTG AGC TGA AGC TA -3`	20

3.6 BBB Integrity

The integrity of the endothelial barrier formed by b.End5 in the co-culture model after passage of the liposomes was determined by TEER measurement, which reflects the dynamic integrity of tight junctions [85]. The TEER reading process was performed as described in [86] . Briefly, TEER was measured using an EndOhmTM chamber coupled to an EVOMX resistance meter (World Precision Instruments, Inc., USA). Readings were registered 0 h and 24 h after liposomes incubation. The value of the empty insert was removed from the TEER values in each condition and multiplied by the insert area (1.12 cm^2). The values from TEER were normalized for the control and expressed as a fold-change for the 0 h of co-culture.

3.7 Statistical and data analysis

Results were analyzed using GraphPad Prism® 8.0 (GraphPad Software) and are expressed as mean ± SEM of three independent assays. The LD50 of SAL was quantified by generating 7-point dose response curves, as described above ranging from 0.1 to 160 µM. LD50 values were calculated by fitting data to the standard four parameter sigmoidal dose response curve. In immunofluorescence, 10 images were acquired for each assay and were treated using ImageJ and Icy software.

IV. Results

4.1 Effect of CTX-siPDGF-B-SNALPs in PDGF-B expression in tumor cells

Preliminary studies carried out in the Neurovascular Laboratory group have demonstrated the efficiency of encapsulation a siRNA in SNALPs, as well as its physical-chemical characterization (Joana Godinho-Pereira, PhD thesis, Faculdade de Farmácia, Universidade de Lisboa, ongoing). CTX-siRNA-SNALPs were already characterized, showing an average size of 120 nm and neutral charge, and around 70% siPDGF-B encapsulation efficiency. Once we had characterized liposomes, the first step was to study the effect of CTX-siPDGF-B-SNALPs on 4T1 cell. To this end, different concentrations (10 and 50 nM) of siScramble and siPDGF-B were studied to assess whether CTX-siPDGF-B-SNALPs exhibited toxicity to 4T1 cells and silenced PDGF-B expression. For this, 4T1 cells were incubated with CTX-siPDGF-B-SNALPs for 24 h, and the viability was determined by the resazurin assay, while PDGF-B expression was determined by the RT-qPCR, both represented in **Figure 4.1**.

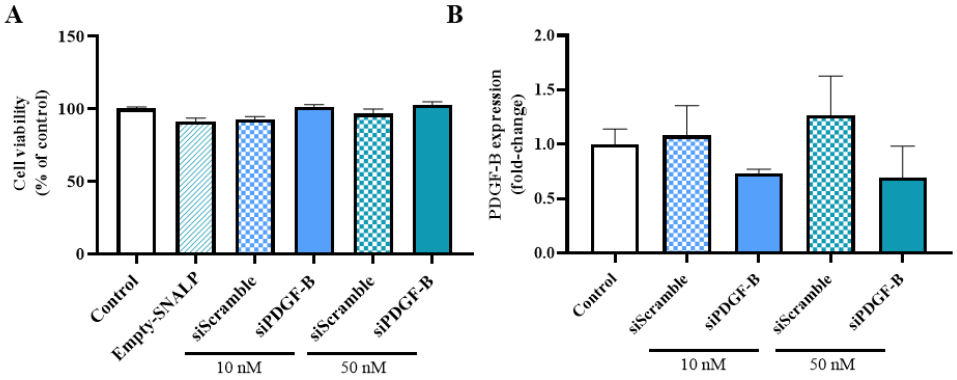

Figure 4.1 4T1 cells' viability and PDGF-B expression by CTX-siPDGF-B-SNALPs exposure 4T1 cells were treated with different concentrations of siScramble and siPDGF-B in liposomes as well as with empty liposomes equivalent to the highest lipid concentration in siPDGF-B liposomes or DMEM (control) for 24 h. (**A**) Cell viability, assessed by the resazurin assay, demonstrated no effect of liposomes on 4T1 cells' viability. The values are presented as percentages relative to the control. (**B**) PDGF-B expression was determined by RT-qPCR. Liposomes showed a tendency to decrease PDGF-B expression, reaching 31% with 50 nM siPDGF-B. Values are shown as fold-change vs control. All values are mean ± SEM of three independent experiments. Statistical analysis was performed by one-way ANOVA.

It was observed that all conditions and both concentrations tested do not show toxicity to tumor cells (**Figure 4.1A**). Next, the effect of CTX-siPDGF-B-SNALPs on PDGF-B expression was evaluated to determine the optimal concentration to follow for the remaining assays, as shown in **Figure 4.1B**. With a concentration of 10 nM of siPDGF-B, it was obtained a silencing of approximately 27%, that increased to around 31% when the concentration was increased to 50 nM. We also demonstrated that siScramble concentrations do not influence PDGF-B expression compared to the control, which indicates a specific silencing. Hence, the concentration of 50 nM was chosen to proceed with further studies.

4.2 Salinomycin-incorporated liposomal formulation

4.2.1 Salinomycin incorporated assay

An initial goal of this work was to co-encapsulate SAL with siPDGF-B. Therefore, a study of the co-encapsulation efficiency of SAL in a SNALPs was carried out (**Table 4-1).**

Table 4-1 Summary of salinomycin encapsulation in SNALPs' conditions and properties

Formulation	z-average (nm)	PdI	IE_{SAL} (%)
A	104	0.210	0.04
B	177	0.242	0.12
C	111	0.185	0.60

PdI: polydispersity index, IE: incorporation efficiency, SAL: salinomycin

To co-encapsulate both SAL and siPDGF-B, an attempt to incorporate the drug into the lipid bilayer of SNALPs composed by DODAP:DSPC:Chol:PEG (25:22:45:8, % molar ratio to total lipid; formulation A) was made. Through analysis of the amount of SAL by UHPLC-MS/MS, and by calculating the IE of the drug, we obtained an incorporation efficiency of approximately 0.04%. Due to the poor IE, a second test was performed (formulation B), where the lipid ratios were changed to 25:45:22:8, % molar ratio to total lipid, in order to understand if the amount of Chol influences the success rate of drug incorporation. Indeed, a marginally increase was observed (0.12%). When adding siRNA to the system (formulation C) the IE only increased to 0.60%. These results show that co-encapsulating SAL and siRNA was not feasible within our system.

Once co-encapsulation proved not to be possible, it was necessary to move on to the contingency plan, which consists of the co-administration of two liposomes, one with siRNA and the other with SAL. For incorporation of SAL alone, several formulations with different lipid compositions and concentration were prepared and their physical properties were determined (formulation D-M), as show in **Table 4-2.**

Firstly, the lipid composition DSPC:Chol:PEG (formulation D and G) and EPC:Chol:PEG (formulation E and F), at a molar ratio of 85:10:5, were studied with different initial lipid concentration (13 or 26 µmol/mL, respectively). The main difference between the formulation D and E is the fluidity of the resulting lipid bilayer (rigidity<DSPC<EPC<fluidity). Similarly, to SNALP, SAL was dissolved with lipids to be incorporated in the lipid bilayer. The four formulations tested showed an IE between 1.78 and 8.68%. The efficiency increased when the total lipid concentration was 26 µmol/mL, so this concentration was selected for the following tests. Next, the effect of using a chemical analogue of Chol, CHEMS (formulation H) was studied. This formulation composed by DOPE:CHEMS:DMPC:PEG (37.5:20:37.5:5 % molar ratio), did not lead to an IE increment (4.80%). Further, the influence of charge on drug incorporation was tested. For that, 3 formulations (I, J, K) were developed using an anionic lipid (I- DPPC:DPPG:PEG; J- DMPC:DMPG:PEG; K-DOPC:DOPG:PEG, all at a molar ratio of 85:10:5), and different structural lipids that differ in their fluidity. In this set of formulations, IE increased to 7.87%, 9.51% and 14.89%, respectively. Even so, in an attempt to further enhance the incorporation of

SAL, and since Chol content may influence the process, as it is found in the lipid bilayer [87] in the same space as SAL, initial formulations composed only by DSPC and EPC were studied. The L formulation (DSPC:PEG - 95:5 % molar ratio) did not reach the end of the process as it jellified, precluding the use of this lipid composition. Finally, the formulation M (EPC:PEG - 95:5 molar % ratio) reached the end of the process and had a SAL IE of 17.83%. Therefore, M formulation was the one chosen to proceed to the remaining work.

Table 4-2 Summary of the conditions tested during salinomycin liposomes development and physical properties

Formulation	z-average (nm)	PdI	IE_{SAL} (%)
D	126	0.059	1.78
E	129	0.053	3.65
F	135	0.044	6.94
G	119	0.062	8.68
H	115	0.052	4.80
I	115	0.059	7.87
J	103	0.057	9.51
K	131	0.058	14.89
L	-	-	-
M	124	0.052	17.83

PdI: polydispersity index, IE: incorporation efficiency, SAL: salinomycin

4.2.2 Salinomycin liposome optimization

After selecting the formulation, the liposome development process was optimized using the DRV method. This method was used to increase the IE of SAL, being tested several times to improve and optimize the procedure. The resulting SAL-Lip characterization is shown in **Table 4-3**.

Table 4-3 Salinomycin-loaded liposome characterization

Formulation	z-average (nm)	Lip_i (µmol/mL)	Lip_f (µmol/mL)	SAL_i (µg/mL)	SAL_f (µg/mL)	IE_{SAL} (%)	LC_{SAL} (µg/µmol)
EMP-Lip	127 ± 4	22.9 ± 1.9	16.2 ± 2.3	-	-	-	-
SAL-Lip	117 ± 9	23.1 ± 2.0	16.2 ± 3.11	3283	697.5 ± 365.1	33.1 ± 21.4	44.8 ± 23.8

SAL: salinomycin, Lip: liposome, Emp: empty, IE: incorporation efficiency, LC: loading capacity

The formulation resulting from the various tests had an average size of 126.6 nm (empty) and 117.4 nm (SAL). During the process of liposome formation, there was some lipid loss associated with the procedure. The concentration of SAL incorporated in the liposomes was improved when the formulation was prepared by the DRV method, achieving an IE of 33.1% and an LC of 44.8 µg/µmol. Thus, having chosen the lipid composition, and having optimized the process of liposome preparation, the next step consisted of the insertion of the peptide into the liposome surface in order to specifically deliver the liposome to the tumor cells.

4.2.3 Targeted salinomycin liposome characterization

After optimizing the development of the formulation, we proceeded to couple CTX to the liposome surface through post-insertion method. Several different tests were carried out to optimize the parameters. After optimizing the functionalized liposome, its physicochemical characterization was carried out, by measuring the z-average, as well as by calculating the IE % and the LC of SAL and IC for CTX. The characterization achieved is represented in **Table 4-4**.

Table 4-4 CTX-salinomycin-loaded liposome characterization

Formulation	z-average (nm)	IE_{SAL} (%)	LC_{SAL} (µg/µmol)	CTX (µmol/mL)	IC_{CTX} (nmol/µmol)
CTX-EMP-LIP	183 ± 32	-	-	0.053 ± 0.0014	4.9 ± 0.17
CTX-SAL-LIP	163 ± 40	73.3 ± 4.2	59.8 ± 4.2	0.065 ± 0.0013	5.4 ± 0.51

SAL: salinomycin, Lip: liposome, Emp: empty, IE: incorporation efficiency, LC. loading capacity; IC: insertion capacity

The liposomal formulations before post-insertion showed an average size of 117.4 nm with SAL and 126.6 nm without. Their median size increased to an average of 163.1 nm with SAL and 182.5 nm without, after adding CTX to their surface. The PdI and the z-potential were determined for all liposomes prepared, to establish the homogeneity of the populations, as well as their charge. Non-functionalized liposomes had a PdI of less than 0.1, while functionalized liposomes approached the value of 0.2. Due to the presence of PEG on the surface of the liposomes (non-functionalized and functionalized) the zeta potential presented a neutral value corresponding to a neutral vesicle. To overcome the long quantification time of SAL, this was performed in non-functionalized liposomes. In CTX-SAL-Lip, SAL was quantified indirectly from the amount of lipid loss. After all the optimization processes, it was obtained an IE of 73.3%, corresponding to 59.8 µg SAL/µmol of lipid. Through quantification of the surface CTX, it was concluded that the presence of SAL in the lipid bilayer did not influence the post-insertion process. In empty liposomes, we obtained an average of 4.9 nmol of CTX per µmol of lipid, while in SAL liposomes the value was 5.4 nmol of CTX per µmol of lipid. It should be noted that the ratio of CTX/lipid was higher than the theoretical 4 nmol/µmol [29], since the amount of CTX to be added was determined based on the initial lipid concentration, which suffers losses during the process.

4.3 Effect of salinomycin in cell viability of tumour cells

To establish the effect of SAL in BCCs viability, 4T1 cells were incubated for 24 h with different concentrations of SAL (free and incorporated) and cell viability was determined by the resazurin assay. Moreover, the LD50 of the drug under each of the conditions was calculated based on 7-point dose response curves. The results obtained are shown in **Figure 4.2.**

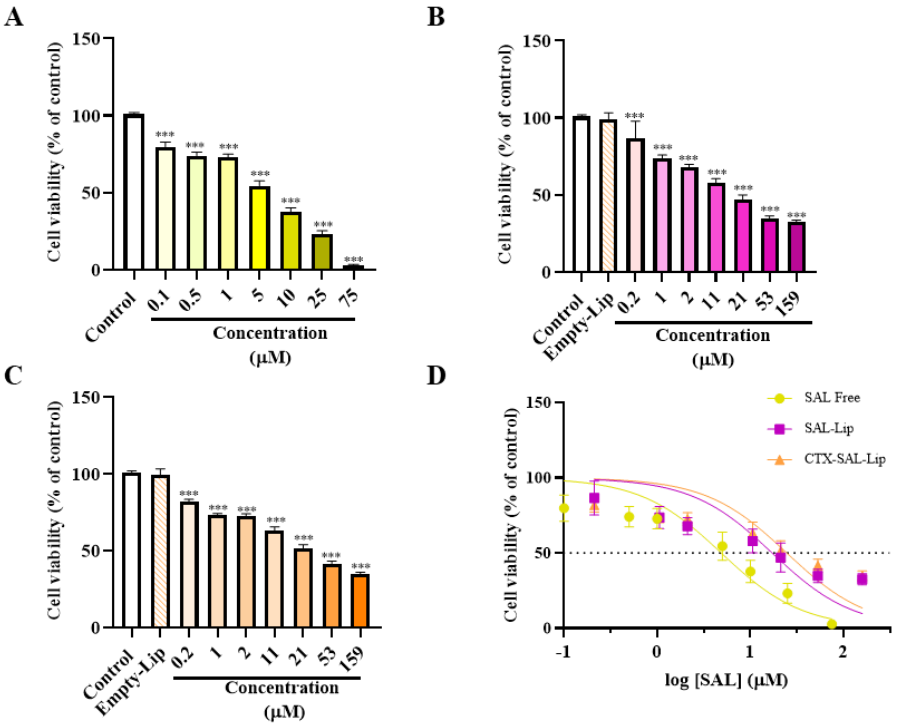

Figure 4.2 Evaluation of 4T1 cell viability upon incubation with free SAL and SAL-loaded liposomes. 4T1 cell line were treated with different concentrations of SAL (free, liposome, and targeted liposome), as well as with empty liposomes equivalent to the highest lipid concentration in the SAL-loaded liposomes. Cell viability was determined by the resazurin assay for (**A**) SAL free, (**B**) liposome with SAL, and (**C**) targeted liposome with SAL. (**D**) The median lethal dose (LD50) SAL was quantified by generating 7-point dose response curves. LD50 values were calculated by fitting the data to the standard four parameter sigmoidal dose response curve. The values are presented as percentage relative to the negative control (untreated cells). SAL significantly decreased cell viability in a dose-dependent manner in all conditions. Values are mean ± SEM of three independent experiments performed in triplicate. Statistical analysis was performed by one-way ANOVA. Significance was shown as ***p<0.001 vs. control.

As shown in **Figure 4.2.A**, SAL (0.1 to 75 µM) decreased cell viability in a dose-dependent manner with almost total loss of cell viability with the concentration of 75 µM. Then, cells were incubated with different concentrations of SAL-loaded liposomes, to understand the effect of the drug incorporation on cell viability. Knowing that drug incorporation usually increases the concentration necessary to obtain the same effect as the free drug, a higher concentration range (0.2 to 159 µM) was studied. Again, a concentration-dependent effect on cell viability was observed, though less drastic than with free SAL (**Figure 4.2B)**. Finally, the study of the effect of functionalized liposomes on cell viability revealed a profile similar to non-functionalized liposomes **(Figure 4.2C)**. To study the eventual contribution of the lipids in the observed toxic effect, an equivalent lipid concentration to the highest SAL dose used was tested with empty liposomes. As shown in **Figure 4.2B-C**, liposomes without SAL did not affect the viability, indicating that the observed viability impairment was due to the drug. The LD50 analysis under different conditions revealed that the LD50 values were 4.87 µM, 17.94 µM and 24.76 µM, for free SAL, SAL-Lip and CTX-SAL-Lip respectively (**Figure 4.2D**). This demonstrates that higher concentrations of SAL are required to obtain more than 50% cell death upon incubation with SAL in liposomes.

4.4 Effect of co-administration in tumor cells

Having studied CTX-SAL-Lip and CTX-siPDGF-B-SNALPs effects alone, our next step was to verify whether the co-administration of both formulations was beneficial. For that, 4T1 cells were incubated

with CTX-SAL-Lip (corresponding to 25 µM of SAL) and/or CTX-siPDGF-B-SNALPs (with 50 nM of siPDGF-B), and both viability and PDGF-B expression were determined (**Figure 4.3)**.

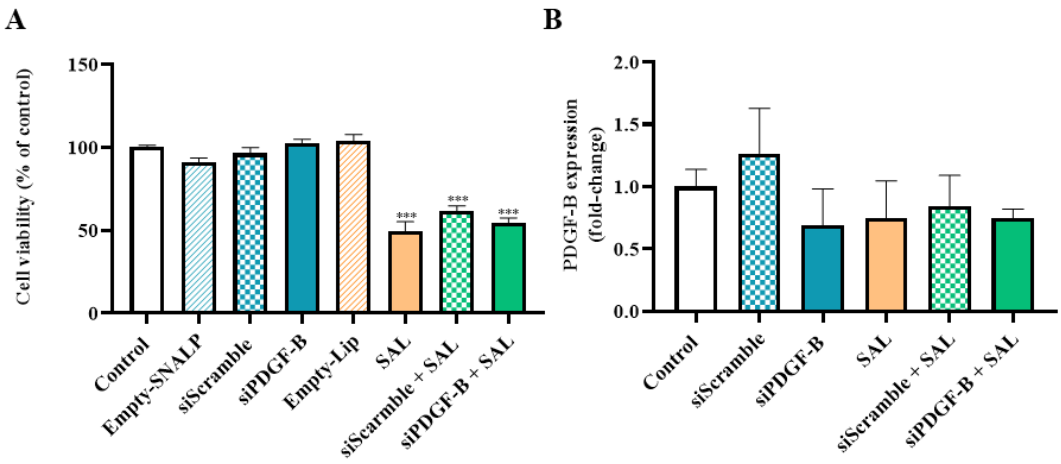

Figure 4.3 Evaluation of 4T1 cell viability and PDGF-B expression upon co-incubation with CTX-siPDGF-B-SNALPs and CTX-SAL-Lip. 4T1 cells were treated with siPDFG-B and/or SAL in liposomes, as well as with empty liposomes with a lipid concentration equivalent to the lipid concentration in siPDGF-B and SAL liposomes, or DMEM for 24 h. (**A**) Resazurin assay demonstrates that CTX-SAL-Lip presents an effect on 4T1 cells' viability, decreasing it in 50 %. The values are presented as percentage relative to the negative control. (**B**) PDGF-B expression was determined by RT-qPCR, showing a decrease in expression when cells were treated with liposomes with siPDGF-B and/or SAL. Values are shown as fold-change vs control. All values are mean ± SEM of three independent experiments. Statistical analysis was performed by one-way ANOVA. Significance is shown as ***p<0.001 vs. control.

As observed in sections 4.1 and 4.3, liposomes with siPDGF-B, siScramble or empty showed no effect on 4T1 cell viability, whereas liposomes with 25 µM SAL decreased cell viability by 50%. With co-administration no increment on cell toxicity was observed, maintaining it at 50% **(Figure 4.3A)**, which was expected since PDGF-B does not directly affect the metabolic capacity of the cell but instead other cellular processes. The expression of PDGF-B (**Figure 4.3B**) was unaffected in control or liposomes with siScramble-treated cells, while encapsulated siPDGF-B treatment demonstrated a decreased PDGF-B expression by about 31%. Of interest was the observation that PDGF-B expression was also affected by SAL, as indicated by the similar decreased expression of the growth factor in cells treated with liposomes with SAL or a with a combination of liposomes with siScramble and liposomes with SAL. Moreover, a decrease of PDGF-B expression by around 25% was observed with the co-administration of encapsulated siPDGF-B and SAL not surpassing the individual effect of each molecule.

4.5 Influence of CTX-siPDGF-B-SNALPs and CTX-SAL-Lip on tumor cells proliferation

As mentioned above, PDGF-B was shown to be upregulated in BCCs and was associated with their proliferation [23, 26]. It has also been mentioned that SAL affects various tumorogenic processes [62]. Thus, to understand whether PDGF-B silencing and SAL affected the profileferative properties of tumor cells, 4T1 cells were incubated with CTX-siPDGF-B-SNALPs (50 nM of siPDGF-B) and/or CTX-SAL-Lip (25 µM of SAL) for 24 h, and the proliferation marker, Ki-67, was analysed (**Figure 4.4)**.

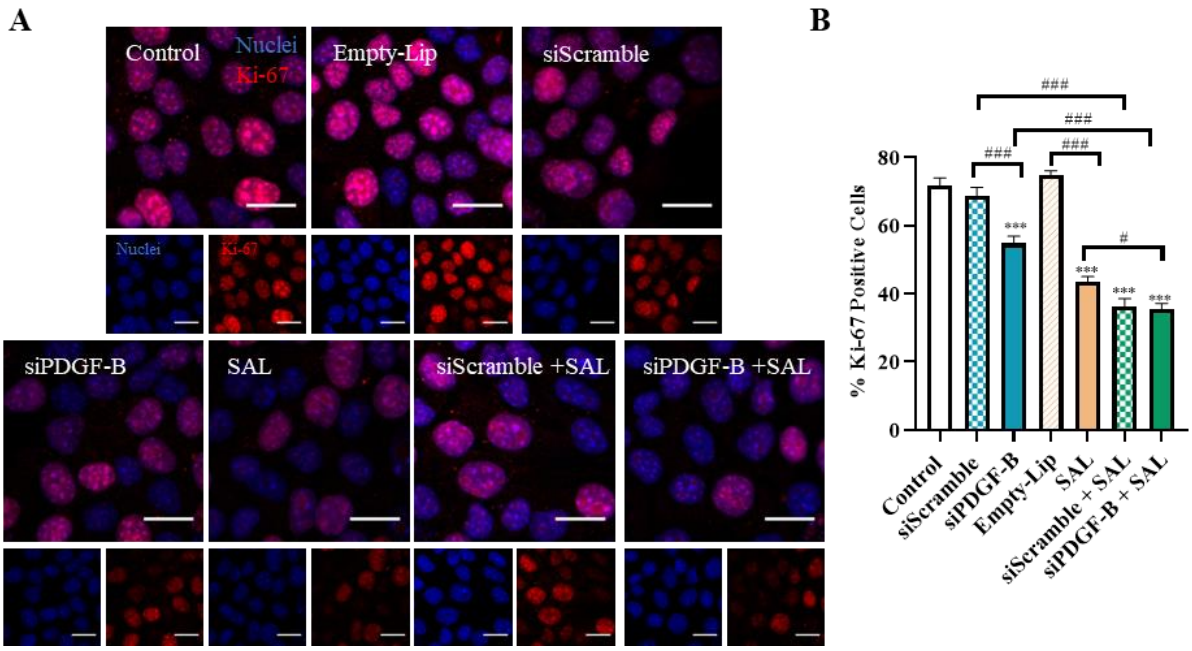

Figure 4.4 Influence of the CTX-siPDGF-B-SNALPs and/or CTX-SAL-Lip on the proliferative properties of 4T1 cells. 4T1 cells were treated with siPDFG-B, or siScramble, and/or SAL in liposomes, as well as with empty liposomes with a lipid concentration equivalent to the lipid concentration in SAL liposomes, or DMEM (control) for 24 h. (**A**) The proliferative properties of 4T1 cells were evaluated by immunofluorescence analysis of Ki-67 (red), demonstrating that CTX-siPDGF-B-SNALPs and CTX-SAL-Lip decreased the proliferative properties. Scale bar: 20 µm. Counterstaining with Hoechst 33342 dye. (**B**) The percentage of Ki-67 positive cells was quantified and showed a decrease with siPDGF-B, SAL, and both formulations compared with the control, siScramble and Empty-Lip. Values are expressed as mean ± SEM of three independent experiments. Statistical analysis was performed by one-way ANOVA. Significance is shown as ***p<0.001 vs. control and # p<0.05, and ###p<0.001 between the indicated conditions.

Qualitative analysis of Ki-67 intensity, revealed a decrease in its expression when cells were treated with SAL formulation and/or siPDGF-B formulation **(Figure 4.4A)**. In the control (cell were not tretaed with liposomes), or in cells treated with liposomes with siScramble or with Emp-Lip, it was noticed that more than half of the cells present an intense red stain, indicating that they have a high amount of Ki-67. On the other hand, after incubation with liposomes containing siPDGF-B, we observed that only half of the cells show an intense red stain. When cells were incubated with SAL or co-incubated with liposomes carring siPDGF-B or siScramble, it was observed that less than half of the cells show an intense red stain. This indicates that both liposomes have the capacity to decrease the proliferation of 4T1 cells. These results were confirmed by semi-quantitative analysis of Ki-67 positive cells (**Figure 4.4B)**. For this, a threshold was established and the cells were divided into positive or negative. Control cells had 72% positive cells for Ki-67, while cells incubated with siScramble-loaded liposomes had 69% positive cells, showing no significant differences between the two groups. However, 4T1 cells treated with CTX-siPDGF-B-SNALPs showed significant differences versus control and siScramble, decreasing the number of Ki-67 positive cells to 55%. The study of the cells incubated with CTX-Emp-Lip demonstrated that 75% of the cells were positive to Ki-67, while incubation with CTX-SAL-Lip alone led to only 43% of positive cells. The co-administration of both CTX-siPDGF-B-SNALPs and CTX-SAL-Lip formulations revealed a significant decrease in Ki-67 positive cells compared to the single use of either one of the liposome, with only 35 % of Ki-67 positive cells. This way, our results show that PDGF-B silencing and SAL treatment decrease 4T1 cell proliferation.

4.6 Safety of nanoformulations for endothelial cells

Up to now it was demonstrated that the co-administration of the two developed formulations not only caused toxicity in tumor cells, but also decreased the expression of PDGF-B and proliferation. Therefore, the use of this approach emerges as a potential new treatment for BCBM. However, for this, the formulations must have the ability to cross the BBB and act on the BCCs in the brain parenchyma, without causing toxicity to resident cells, like endothelial cells. For that, b.End5 cells were incubated with different concentrations of SAL free or CTX-SAL-Lip or CTX-siPDGF-B-SNALPs for 24 h and cell viability was studied by the resazurin assay. Results are shown in **Figure 4.5.**

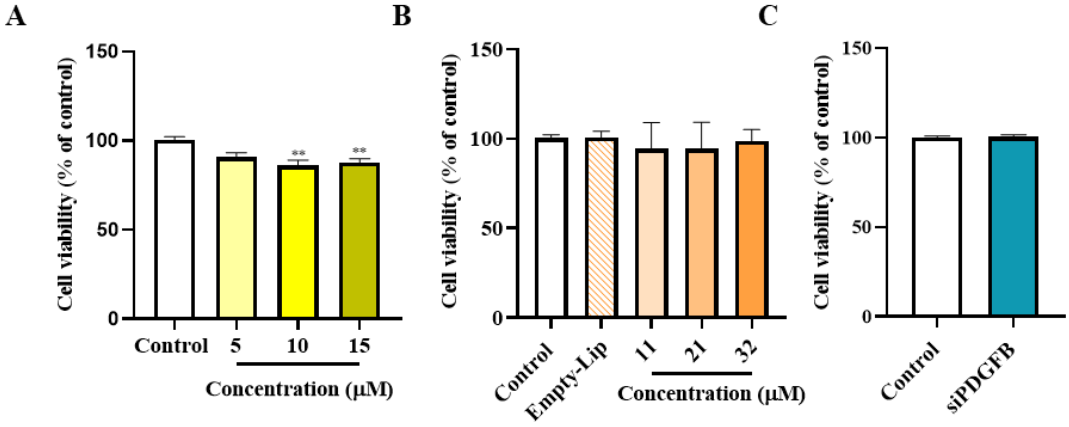

Figure 4.5 CTX-siPDGF-B-SNALPs and CTX-SAL-Lip safety profile for b.End5 cells. (**A, B**) b.End5 cells were treated with different concentrations of SAL (free and targeted liposomes), as well as with empty liposomes with a lipid concentration equivalent to the highest in the SAL liposomes, or DMEM (control) for 24 h. Cell viability was assessed by the resazurin assay for (**A**) free SAL and (**B**) targeted liposomes with SAL. Free SAL decreased cell viability, whereas incorporated SAL showed no signs of toxicity to b.End5 cells. (**C**) b.End5 cells were treated with 50 nM of siPDGF-B or no addition (control), for 24 h. Liposomes showed no effect on cell viability. The cell viability is presented as percentage relative to control cell and is expressed as mean ± SEM of three independent experiments performed in triplicate. Statistical analysis was performed by one-way ANOVA. Significance is shown as **p<0.01 vs. control.

Concentrations greater than 10 µM of SAL in its free form demonstrated a small reduction in the viability of b.End5 cells (**Figure 4.5A)**. However, when incorporating SAL in liposomes, concentrations greater than 10 µM have not been shown to significantly affect endothelial cell viability (**Figure 4.5B)**. This way, the results indicate that the use of liposomes to deliver SAL was beneficial, as we can affect the viability of tumor cells without affecting viability of endothelial cells, unlike the free drug. The effect of the lipid composition of the liposome (empty liposome) was also studied, not impacting b.End5 cells' viability. The safety of CTX-siPDGF-B-SNALPs was also studied (**Figure 4.5C)**, demonstrating that the formulation was safe for the endothelium.

4.7 Effect of co-administration in a co-culture model

After confirming that CTX-siPDGF-B-SNALPs and CTX-SAL-Lip presented no effect on endothelial cells' viability, the last step of the work was to study the co-administration in a co-culture model that mimics BCBM **(Figure 4.6)**. The co-cultures are necessary to evaluate liposomes` BBB transposition efficiency and efficacy to act upon the BCCs (in the "brain side"), and to determine the BBB integrity during the passage of liposomes. In this co-culture model, b.End5 cells were seeded on semi-permeable membranes and liposomes were applied to them (from the "blood side") in order to pass through the barrier and act on 4T1 cells, seeded in the lower compartment ("brain side"), as illustrated in **Figure**

4.6A. After 24 h of incubation, the expression of PDGF-B and p16 (senescence marker) were studied. Furthermore, liposomes safety to BBB was established by TEER measurement.

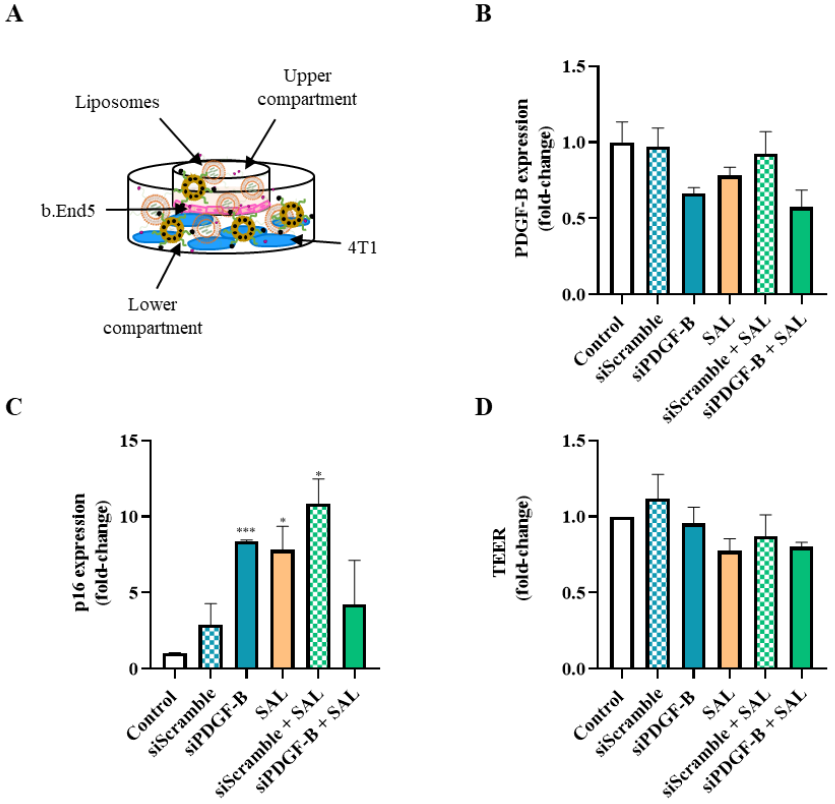

Figure 4.6 CTX-SAL-Lip or CTX-siPDGF-B-SNALPs's blood brain barrier transposition efficacy in a co-culture model and its action on 4T1 cells. (**A**) b.End5 cells were seeded onto a semi-permeable membrane (Transwell inserts) with the luminal surface facing the upper compartment ("blood" side) and BCCs were plated on the bottom of the cell culture plate ("brain" side). Liposomes were administered in the upper ("blood") compartment and after 24 h their effect in 4T1 cells was evaluated. (**B, C**) The expression of PDGF-B and p16 were evaluated through RT-qPCR and the values are shown as fold change vs control. (**B**) CTX-siPDGF-B-SNALPs or CTX-SAL-Lip, and their combination, decreased PDGF-B expression. (**C**) Liposomes with SAL or siPDGF-B promoted the upregulation of the senescence markers p16. (**D**) The liposomes' effect on BBB properties was assessed by transendothelial electrical resistance (TEER), an indicator of BBB's integrity, before (0 h) and after (24 h) of liposomes addition. The values from TEER were normalized for the control and expressed as a fold-change for the 0 h of co-culture. Data are mean ± SEM of three independent experiments, and statistical analysis was performed by one-way ANOVA and Student´s t-test. Significance was shown as *p<0.05 and ***p<0.001 vs. control.

As shown in **Figure 4.6B**, no changes in PDGF-B expression after incubation with liposomes with siScramble or in control cells were observed. When incubated with CTX-siPDGF-B-SNALPs a 34% silencing of the expression of the growth factor was observed. Interestingly, cells incubated only with CTX-SAL-Lip also revealed a decrease in PDGF-B expression, though with a lower magnitude (22%). The co-administration resulted in a silencing of 43%. These results indicate that both formulations can cross the BBB and act on the BCCs, impairing the growth factor expression.

Finally, it was studied whether siPDGF-B and/or SAL induced 4T1 cells senescence. To this end, the expression of p16, cell cycle arrest marker [88], was assessed. By analyzing **Figure 4.6C** we observe that cells treated with encapsulated siScramble have a slight increase in p16 expression. Cells treated only with liposomes containing siPDGF-B or SAL, demonstrate a significant increase of about 8x and 7x, respectively. Furthermore, co-administration of liposomes with siScramble and SAL reveals an increase in p16 no significative compared to the individual liposomes. Finally, incubation with siPDGF-B and SAL reveals a tendency to increase in relation to the control, and to decrease in relation to siScramble+SAL. Our results indicate that both liposome formulations (siPDGF-B or SAL) promote cell senescence, with no increase in the effect of co-administration in promoting senescence.

Next, BBB integrity was studied by the TEER. Although no significant variations in each of the tested conditions compared to the control were observed (**Figure 4.6D**), TEER values decreased by around 20% after the passage of liposomes containing SAL, which raises concerns about BBB integrity.

4.8 Effect of co-administration in endothelial barrier

To in-depth depict the impact of SAL-loaded liposomes in the BBB, analysis of the expression of β-catenin, an important protein in the BBB junctions and indicator of barrier integrity [89], was performed. To process this, b.End5 cells were incubated with CTX-siPDGF-B-SNALPs (50 nM of siPDGF-B) and/or CTX-SAL-Lip (25 µM of SAL) for 24 h and β-catenin staining was assessed by immunofluorescence (**Figure 4.7)**.

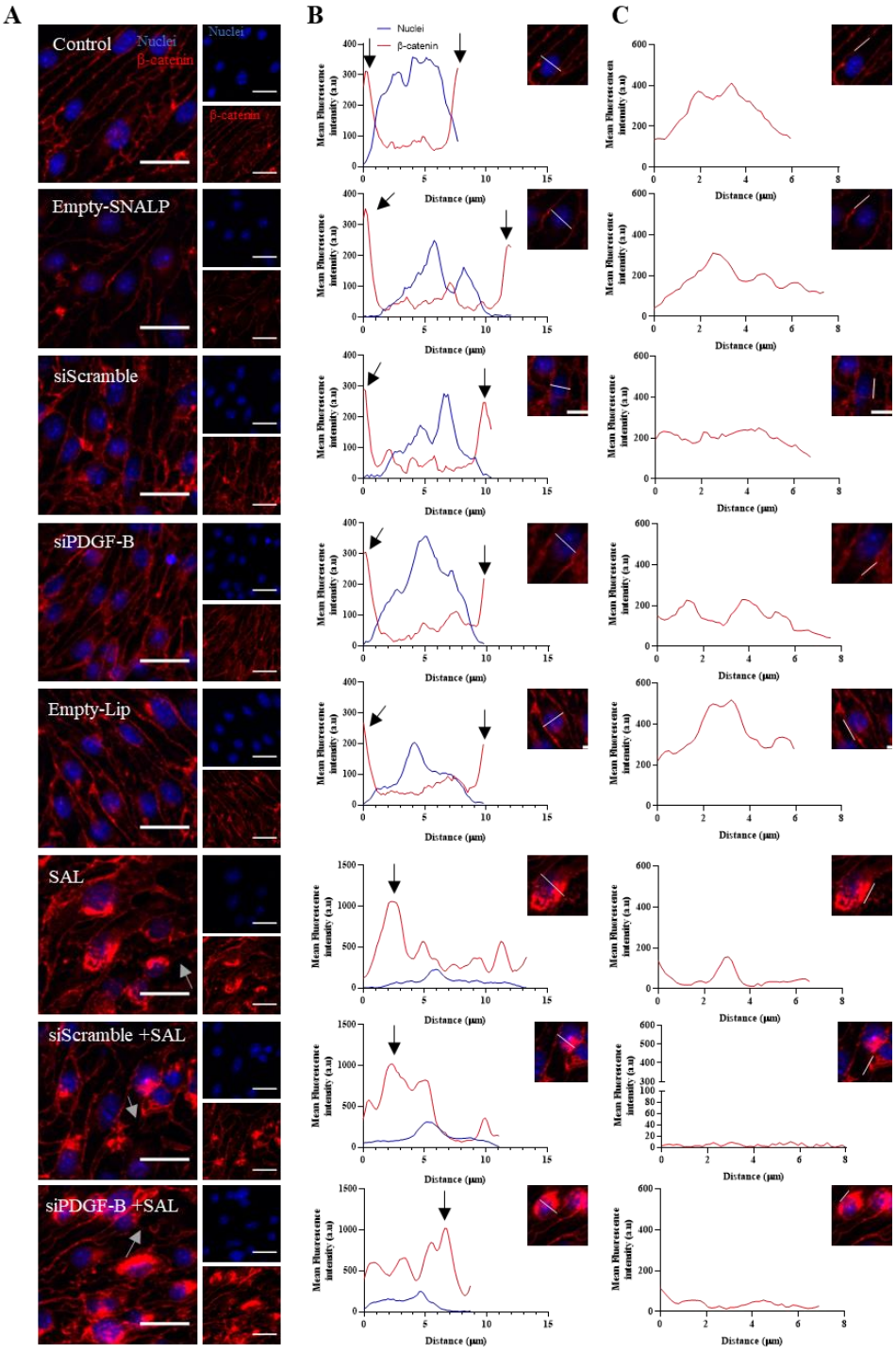

Figure 4.7 b.End5 barrier integrity after treatment with CTX-SAL-Lip or CTX-siPDGF-B-SNALPs b.End5 cells were treated with siPDFG-B, siScramble and/or SAL in liposomes, as well as empty liposomes with a lipid concentration equivalent to the lipid concentration tested in siPDGF-B and SAL liposomes, or DMEM (control), for 24 h. (**A**) The integrity of b.End5 monolayers was evaluated by immunofluorescence analysis of the adherens junction protein, β-catenin (red), which demonstrated that CTX-SAL-Lip impairs its integrity, leading a delocalization of β-catenin, with appearance of "holes" in the endothelial cell membrane (gray arrows). Scale bar: 20 µm. Counterstaining with Hoechst 33342 dye. (**B**) The localization of β-catenin was studied through plot profile of pixel intensity troughout an endotelial cell (edge to edge, as shown in the crop), demonstrating that in control, empty liposomes and liposomes with either siScramble or siPDGF-B, the intensity peaks of β-catenin were found at the edges of the cells (black arrows) correspondingto the cell membrane. While under conditions incubated with CTX-SAL-Lip it was possible to observe both an increase in fluorescence intensity as well as an increase in β-catenin localization in the perinuclear region (black arrows). (**C**) The intensity of β-catenin at the membrane was also studied through plot profile of pixel intensity, as represented in the crop. These results once again demonstrate that the intensity of β-catenin present in the membrane decreases in the conditions incubated with SAL when compared to the other conditions studied.

Qualitative analyses of β-catenin (**Figure 4.7A)** revealed that SNALPs encapsulating siScramble or siPDGF-B, as well as Empty-Lip and Empty-SNALPs, do not induce changes in the protein expression profile compared to the control. In contrast, cells incubated with CTX-SAL-Lip, CTX-siScramble-SNALPs/CTX-SAL-Lip and CTX-siPDGF-B-SNALPs/CTX-SAL-Lip revealed differences in the monolayer profile, with a delocalization of β-catenin from the membrane to the cytosol and particularly to the perinuclear region, with appearance of "holes" in the endothelial cell membrane, compatible with a barrier disruption. These results were confirmed by the plot profiles analysis of β-catenin location which showed that in all conditions without SAL (control, liposomes with siScramble or siPDGF-B, Empty-SNALPs and Empty-Lip) the highest intensity was at the membrane (**Figure 4.7B**). However, under the conditions in which liposomes with SAL were present, it was observed that the peak intensity of β-catenin was closer to the peak intensity of the nuclei, accompanied by a mean fluorescence intensity increase. These results show that SAL promotes the accumulation of β-catenin in the perinuclear region. Furthermore, the analysis of the intensity of β-catenin within the membrane was carried out (**Figure 4.7C)**. It was found once again that the conditions with encapsulated siScramble, siPDGF-B, Empty-SNALPs and Empty-Lip are similar to the control, where the intensity of β-catenin was homogeneous across the membrane. In conditions with incorporated SAL, it was observed a decreased intensity of β-catenin in the membrane, almost reaching null values. These results indicate a deficiency in membrane β-catenin expression, causing "hole" along the membrane staining. In summary, these results suggest that CTX-SAL-Lip, despite not causing toxicity to endothelial cells or inducing a statistically significant decrease of TEER values, leads to disruption of the endothelial barrier.

V. Discussion

BCBM patients have a poor prognosis due to the limited therapeutic options and restricted BBB permeability. When BM are diagnosed, patients have an average of less than 1 year to live, with only 20% reaching 1 year [90]. Therefore, innovative therapeutics are needed. These prompted us to develop a groundbreaking treatment that combines molecular and genetic therapies through nanomedicines targeting BCCs to abrogate BCBM.

Our research group has shown that the increase of BM formation associated with TNBC was related with an increase of PDGF-B expression [23]. Therefore, SNALPs encapsulating siPDGF-B were developed to decrease the growth factor expression. An initial screening of the optimal siPDGF-B concentration was performed. SNALPs (empty, siScramble, and siPDGF-B) were shown to have no effect on 4T1 cell viability, which was expected since PDGF-B is a growth factor involved in cell invasion, tumor progression, maintenance of EMT, and vascular modulation, among others [23-28]. Nevertheless, the lipid particles proved to be efficient in the delivery of siRNA and reduction of PDGF-B expression. The best silencing rate was achieved when using 50 nM of siPDGF-B.

Once established the SNALPs formulation, we devised efforts to co-encapsulate the cytotoxic drug SAL. In a first attempt to incorporate SAL, we tried to integrate it into the lipid bilayer, since SAL is a hydrophobic drug. Nonetheless, the IE% was negligible (0.04%). Others' studies suggested that the IE% can be affected by the properties of the compound (hydrophobic or hydrophilic) as well as by the content of Chol in the liposomal formulation [87]. In fact, it was shown that an increase in the percentage of Chol is associated with an IE% decrease, due to a competitive action for the incorporation of Chol and drug in the lipid bilayer. This means that liposomes with high Chol content may limit drug incorporation within the lipid bilayer [87]. Knowing that our SNALP formulation have high Chol (45%), the failure in drug incorporation may be due to this fact, which hampers SAL incorporation into the lipid bilayer. A second SAL incorporation test was performed, where Chol concentration was decreased (22%), to test if its presence affected the incorporation of SAL. However, there was no significant increase in SAL incorporation. These results showed that co-encapsulation of siPDGF-B and SAL in our SNALP system is not possible. So, we decided to switch to a co-administration of two NFs, one with the siRNA for PDGF-B and the other with the cytotoxic drug SAL, as a contingency plan.

One of the main problems in incorporating SAL is its hydrophobicity, which renders necessary its incorporation in the lipid bilayer. Several studies have demonstrated the efficient incorporation of SAL in liposomes [77, 78, 91, 92]. The common point in all these studies is liposome composition that includes a main phospholipid (HSPC or EPC) that differ in their fluidity, Chol and PEG on the surface. Based on these reports, formulations D-G were prepared and the IE of SAL was studied. In our experiments, HSPC was replaced by DSPC, a synthetic lipid used in SNALP [93]. With these tests, we intend to study whether the fluid associated with the main phospholipid component affected the incorporation of the drug in the lipid bilayer. In the 4 formulations studied, it was not possible to obtain an effective IE. Although, it determined that the initial lipid concentration of 26 µmol/mL would be the best concentration to continue the studies.

Next, a liposome composed of CHEMS, an analog of Chol, was studied. However, an improvement in SAL incorporation was not observed. Subsequently, the influence of negative charge on SAL incorporation was studied. Studies show that the presence of negative charge in the lipid bilayer allows the encapsulation of a variety of charged drugs and other macromolecules [94]. In addition to the negative charge, several lipids that differ in their fluidity were studied. In this batch of formulations, the SAL IE increased to 7.87%, 9.51% and 14.89%. However, we remain displeased with the results. As mentioned earlier, Chol can affect SAL incorporation [87]. Therefore, in the following studies, Chol was completely removed from the lipid composition of the liposomes. So, liposomes were developed with only DSPC or EPC and PEG. The liposomal formulation composed only with DSPC:PEG and SAL resulted in a gel-like structure that was not possible to extrude. This event may be associated with the absence of Chol since it interferes with the acyl chains of phospholipids [95] and, when absent, the rigidity of the DSPC chains prevents the formation of liposomes with SAL in their membrane. Finally, liposome with EPC:PEG were prepared. EPC is an egg-derived fluid lipid that we have shown to have the greatest effect on SAL incorporation. Despite showing an increase in IE, some optimization processes were necessary to further increase this parameter. One of the changes implemented was the preparation of the liposome by the DRV method. DRV is a simple method of liposome preparation that employs mild conditions and has the ability to efficiently incorporate a wide range of materials. This process is based on controlled dehydration and rehydration to induce liposome fusion [80, 96], and with it, it was possible to double the IE, incorporating 33% of the total drug. The final step to complete our liposomal formulation was to decorate the surface with a moiety to specifically target BCCs cells. The post-insertion method was chosen to insert CTX (a peptide targeting BCCs cells) conjugated to DSPE-PEG-MAL micelles (CTX-DSPE-PEG-MAL). The association and internalization related with this peptide has been demonstrated in other studies [29, 56]. Quin. et al demonstrated that the use of CTX on the surface of liposomes can increase liposomal uptake by 4T1 cells, that express high amounts of

MMP-2. They also showed an increase in the effect of liposomes in cells when using CTX on surface [56]. It was further demonstrated by Costa and colleagues that CTX coupled to SNALP (4 mol% DSPE-PEG-MAL micelles) increases internalization and association in glioblastoma/glioma cells that also express high amounts of MMP-2. Once again they also shown an increase in the treatment effect [29]. Considering that our aim is to treat BCBM, these studies indicate that the choice of CTX to target BCCs is an appropriate and promising one.

Once established the liposomes composition, their cellular effects were assayed. An initial screening was done to determine the concentration of SAL impairing cell viability, and the LD50 of free and incorporated SAL were determined. For 5 µM of free SAL a pronounced decrease by about 50 % in cell viability was demonstrated, which became almost total at 75 µM. As demonstrated by several studies, SAL has the characteristic of causing apoptosis, inhibition of proliferation and inhibition of tumor growth [97, 98], which can be associated with a dysregulation in cell metabolism that can affect the cell viability. When incorporate, the concentrations tested were higher, once the drug is not so freely available to act upon the cells, being necessary its entry into the cell and subsequent release for it to promote an effect. Our results demonstrated that higher concentrations were needed to achieve similar decreases in viability compared to free SAL. Therefore, SAL in liposomes led to about a 5x increase in the LD50 value compared to free SAL. Comparing the LD50 of the targeted and untargeted liposomes, similar profiles were obtained. These results indicate that the choice of SAL to complete the treatment that aims to eradicate BCBM, was wise.

Having determined the concentrations of encapsulated siPDGF-B (50 nM) and SAL (25 uM) to be applied to cells, the next stage of the work consisted in the study of the effect of the co-administration of CTX-SAL-Lip and CTX-siPDGF-B-SNALPs to 4T1 cells. Co-administration of the two lipid formulations did not show an increased effect on cell viability compared with the toxicity caused by each of the formulations alone. PDGF-B expression was also studied, which confirmed that CTX-siPDGF-B-SNALPs decreases PDGF-B expression. Interestingly, a similar decrease in the growth factor expression was also observed by incubation with CTX-SAL-Lip. The co-administration of CTX-siPDGF-B-SNALPs and CTX-SAL-Lip did not demonstrate a greater decrease in PDGF-B silencing, compared with separate treatments. In fact, other studies have shown a decrease in the PDGF-B receptor when cells are treated with SAL [92, 98]. So, the decrease of PDGF-B and its receptor will affect the phosphorylation of downstream targets by the intracellular receptor kinase domain, affecting signaling pathway and consequently affect several biological processes. Several studies have demonstrated that SAL can reduce cyclin D1, promoting an epithelial morphology and affecting cell migration [65, 70-72, 97, 98], while PDGF-B increase cytoskeleton remodeling and cell motility and autocrine PDGF-B signaling contributing to the maintenance of EMT [19, 25]. Another biological process that we have shown to be affected in BCCs treated with CTX-siPDGF-B-SNALPs or CTX-SAL-Lip is cell proliferation. Accordingly, our study of the effects of PDGF-B silencing and SAL on BCCs proliferation showed a decrease in Ki-67 positive cells. Our results agree with Thies et al. which demonstrates that PDGF-B is involved in proliferation [26]. Studies by Wang et al. also demonstrated that SAL leads to cell cycle arrest in G0/G1 and in G1/G2 [67, 99, 100], corroborating our results on SAL-dependent decreased cell proliferation. Although a further decrease in the cell proliferation marker was observed by the co-administration of both liposomes, the fact that a significant decrease was also observed in cells treated with the siScramble, does not allow to conclusively establish that the double treatment has an additive effect in the proliferation of 4T1 cells.

In this type of studies, it is important to determine the safety of liposomal formulations for resident cells like BMECs. Our results have been shown that small concentrations of free SAL lead to a small reduction in BMECs cell viability. This toxicity was lost when cells were incubated with higher concentrations of incorporated SAL. We also proved that siPDGF-B was safe for BMEC. Drug encapsulation in a liposome provides a physical barrier [101, 102] between the drug and the BMECs,

which leads to reduced collateral toxicity associated with the study drug. These results are in line with the aim of the project, which is to deliver SAL and siPDGF-B in a more targeted way and reduce the collateral toxicity associated with these types of treatments.

Having demonstrated the safety of the formulations for the BMECs, co-culture assays were initiated. We found that liposomes have the ability to cross the BBB since the application of liposomes in the upper ("blood") compartment of the inserts had effect on tumor cells in the lower ("brain") compartment. Indeed, decrease in PDGF-B expression was observed when cells were incubated with CTX-siPDGF-B-SNALPs. Furthermore, the expression of PDGF-B upon treatment with incorporated SAL treatment was also reduced. p16 is a tumor suppressor that binds to cyclin-dependent kinases (CDK)4/6 and inhibits the cell cycle in G1, causing the cell to enter a senescent state [88]. Cells treated with liposomes containing SAL or siPDGF-B demonstrate a higher expression of p16. Actually, these results are in line with other studies that demonstrated cellular senescence induced by SAL [92, 97]. For the PDGF-B, as far as we know we are the first to demonstrate that the silencing of PDGF-B causes cell senescence. The co-encapsulation (siPDGF-B+SAL) demonstrated a tendency to decreased senesce compared with siScrambe+SAL. Dhaheri et al. shown that lower concentrations of SAL lead to an increase in p21 [73] (cell cycle inhibitor [103]), while higher concentrations can lead to a decrease in p21 and survivin [73]. As survivin is an inhibitor of apoptosis, a decrease in its expression may demonstrate a sensitization of cells to apoptosis. These results raise the hypothesis that the co-administration of siPDGF-B and SAL in a liposome can lead to a decrease in p16, where cells do not acquire a senescent state but instead there is an induction of cell death mechanism. However, more studies are needed to confirm the hypothesis. Altogether, our results suggest that the administration of CTX-siPDGF-B-SNALPs and/or CTX-SAL-Lip modulate tumorigenic properties, as well as cell viability, proliferation, and senescence, pointing to the potential of a co-administration therapeutic regimen.

During the co-culture, the TEER values were measured, and the BBB's integrity was assured for the liposomes with siScramble and siPDGF-B. Although a statistically significant change was not observed in conditions with SAL, the moderate decrease raised concern about the integrity of the BBB in cells treated with the drug. This was confirmed by the study of β-catenin, which demonstrated a delocalization of the junctional protein from the membrane to the cytosol and particularly to the perinuclear region. The accumulation of β-catenin in the cytoplasm and subsequent translocation to the nucleus is due to the activation of the canonical Wnt pathway [104, 105]. Studies have shown that Wnt pathway signaling activity is required for BBB maturation but is low when the BBB is fully matured [106]. It was also demonstrated that activation of the canonical Wnt pathway in b.End3 cells leads to negative regulation of CD31, an endothelial marker, and upregulation of smooth muscle actin, a migration marker, showing that activation of the Wnt pathway promotes the induction of the transition for mesenchymal and suppression of endothelial markers [106]. All this leads to the hypothesis that SAL causes a destabilization of the BBB, activating the Wnt pathway, which causes translocation of β-catenin to the perinuclear region and loss of endothelial properties, destabilizing the β-catenin function within the cell membrane. Both the tumor and chemotherapy can lead to pro inflammatory niche of cytotoxic cytokines, cytokines that can promote a transient breakdown of tight junction proteins, thereby leading to an increased inflammatory state and affecting BBB integrity [107]. Many cancer treatments have been designed to transiently disrupt BBB, to increase its permeability [108]. One of the chemotherapeutics used in oncology is carboplatin, this drug demonstrates high clearance of brain tissues and suggests a temporary interruption of the BBB during treatment [109]. Other process that leads to BBB disrupting is the BCCs extravasation. Entry of BCCs into the brain leads to a decrease in adherent and tight junction proteins (β-catenin and Claudin-5, respectively). However, Figueira et al. demonstrates that with time it is possible to recover the expression of the junctional proteins [23]. All of these mentioned above suggest the premise that although CTX-SAL-Lip disrupts the BBB junctions, this disruption may be transient. Additionally, Quin et al, demonstrated that the use of CTX on the surface of liposomes leads to a

decrease in the systemic toxicity associated with the free drug [56]. Thus, suggesting that the advantage of using CTX-SAL-Lip over other chemotherapeutic agents is the reduction of side effects by brain resident cells. However more studies are needed to prove that the benefits of using CTX-SAL-Lip are sufficient to overcome the risks caused by the BBB breakdown.

VI. Conclusion and future perspectives

In recent years, the progress of science has contributed greatly to the development of new therapies that manage to increase the quality of life of BC patients. However, the existence of BBB limits the treatment of BCBM, preventing the passage of therapeutic agents. Thus, this project intends to develop a new nanomedicines platform that crosses the BBB and acts on BCCs. In summary, the present study shows the effective incorporation of SAL in a liposome targeted at BCCs. It also demonstrates the advantage of the liposomes with SAL and siPDGF-B to abrogate BCCs. Once we suggest that SAL and PDGF-B silencing may induce a decrease in BM through the downregulation of cell proliferation and upregulation of senescence. Finally, with these results we establish the possibility of developing a groundbreaking therapy to eradicate BCBM. This therapy, if confirmed the benefit of treatment outweighs the risk and that BBB disruption is transient, could lead to an extraordinary advance in neurooncology field, and may increase the average life expectancy, giving a new hope for patients with BCBM.
In the future, it would be necessary to confirm that CTX-SAL-Lip is safe for administration. For this, it is important to study what happens to the cells after the passage of the liposomes, that is, study the expression of junctional proteins (β-catenin and Zonula occludens (ZO) 1) over time to see if there has been a recovery of their normal expression. Assuming a recovery, it would be interesting to evaluate the mechanism of liposomes' entry into BCCs. For that it would be interesting to perform an internalization assay as well as to study the transcellular transport marker (caveolin-1) (suggested mechanism). Next step would be to perform a preclinical study, in a reliable *in vivo* model of preferential formation of metastases in the brain. The *in vivo* studies aim to evaluate the efficiency of the co-administration of siRNA and SAL in eradicating BM associated with TNBC, through the analysis of the number and area of metastases. In *in vivo* studies, it would also be important to confirm the integrity of the BBB, by studying junctional proteins (β-catenin and claudin-5), as well as a marker of BBB disruption (thrombin). It would be interesting to study also the biodistribution of liposomes by binding the liposome to a fluorescent dye. Also, it would be interesting to study the molecular mechanism of action of the therapy through the evaluation of several markers such as Ras homolog gene family member A (RhoA) and Ras-related C3 botulinum toxin substrate 1 (RAC1) (migration), Ki-67 (proliferation), cyclin D1 (cell cycle), β-galactosidase (senescence) and others, such as inflammatory markers. Lastly, it would be important to study the safety in healthy mice treated with NFs or vehicle, by histological analysis of peripheral organs and toxicity indicators in plasma.

VII. References

[1] H. Sung *et al.*, "Global Cancer Statistics 2020: GLOBOCAN Estimates of Incidence and Mortality Worldwide for 36 Cancers in 185 Countries," *CA Cancer J Clin*, vol. 71, no. 3, pp. 209-249, May 2021.

[2] J. R. Sainsbury, T. J. Anderson, and D. A. Morgan, "ABC of breast diseases: breast cancer," *BMJ*, vol. 321, no. 7263, pp. 745-50, Sep 23 2000.

[3] B. Weigelt, Geyer, F. C., & Reis-Filho, J. S. , "Histological types of breast cancer: how special are they?," *Molecular oncology*, vol. 4, no. 3, pp. 192-208, 2010.

[4] E. A. Rakha and I. O. Ellis, "Triple-negative/basal-like breast cancer: review," *Pathology*, vol. 41, no. 1, pp. 40-7, Jan 2009.

[5] T. Custodio-Santos, M. Videira, and M. A. Brito, "Brain metastasization of breast cancer," *Biochim Biophys Acta Rev Cancer,* vol. 1868, no. 1, pp. 132-147, Aug 2017.

[6] W. J. Irvin Jr, & Carey, L. A. , "What is triple-negative breast cancer?," *European journal of cancer,* vol. 44, no. 18, pp. 2799-2805, 2008.

[7] A. Niwinska, M. Murawska, and K. Pogoda, "Breast cancer brain metastases: differences in survival depending on biological subtype, RPA RTOG prognostic class and systemic treatment after whole-brain radiotherapy (WBRT)," *Ann Oncol,* vol. 21, no. 5, pp. 942-8, May 2010.

[8] K. J. Chavez, S. V. Garimella, and S. Lipkowitz, "Triple negative breast cancer cell lines: one tool in the search for better treatment of triple negative breast cancer," *Breast Dis,* vol. 32, no. 1-2, pp. 35-48, 2010.

[9] S. Cattin *et al.*, "Circulating immune cell populations related to primary breast cancer, surgical removal, and radiotherapy revealed by flow cytometry analysis," *Breast Cancer Res,* vol. 23, no. 1, p. 64, Jun 5 2021.

[10] A. Saha, S. K. Ghosh, C. Roy, K. B. Choudhury, B. Chakrabarty, and R. Sarkar, "Demographic and clinical profile of patients with brain metastases: A retrospective study," *Asian J Neurosurg,* vol. 8, no. 3, pp. 157-61, Jul 2013.

[11] W. Cruz-Munoz and R. S. Kerbel, "Preclinical approaches to study the biology and treatment of brain metastases," *Semin Cancer Biol,* vol. 21, no. 2, pp. 123-30, Apr 2011.

[12] K. Altundag *et al.*, "Clinicopathologic characteristics and prognostic factors in 420 metastatic breast cancer patients with central nervous system metastasis," *Cancer,* vol. 110, no. 12, pp. 2640-7, Dec 15 2007.

[13] B. D. Lehmann *et al.*, "Identification of human triple-negative breast cancer subtypes and preclinical models for selection of targeted therapies," *J Clin Invest,* vol. 121, no. 7, pp. 2750-67, Jul 2011.

[14] A. J. Clayton *et al.*, "Incidence of cerebral metastases in patients treated with trastuzumab for metastatic breast cancer," *Br J Cancer,* vol. 91, no. 4, pp. 639-43, Aug 16 2004.

[15] A. S. Achrol *et al.*, "Brain metastases," *Nat Rev Dis Primers,* vol. 5, no. 1, p. 5, Jan 17 2019.

[16] P. S. Steeg, Camphausen, K. A., & Smith, Q. R. , "Brain metastases as preventive and therapeutic targets. ," *Nature Reviews Cancer,* vol. 11, no. 5, pp. 352-363, 2011.

[17] S. J. Kim *et al.*, "Astrocytes upregulate survival genes in tumor cells and induce protection from chemotherapy," *Neoplasia,* vol. 13, no. 3, pp. 286-98, Mar 2011.

[18] I. Witzel, L. Oliveira-Ferrer, K. Pantel, V. Muller, and H. Wikman, "Breast cancer brain metastases: biology and new clinical perspectives," *Breast Cancer Res,* vol. 18, no. 1, p. 8, Jan 19 2016.

[19] N. Lindberg and E. C. Holland, "PDGF in gliomas: more than just a growth factor?," *Ups J Med Sci,* vol. 117, no. 2, pp. 92-8, May 2012.

[20] I. Nazarenko *et al.*, "PDGF and PDGF receptors in glioma," *Ups J Med Sci,* vol. 117, no. 2, pp. 99-112, May 2012.

[21] P. H. Chen, X. Chen, and X. He, "Platelet-derived growth factors and their receptors: structural and functional perspectives," *Biochim Biophys Acta,* vol. 1834, no. 10, pp. 2176-86, Oct 2013.

[22] L. Uhrbom, G. Hesselager, M. Nister, and B. Westermark, "Induction of brain tumors in mice using a recombinant platelet-derived growth factor B-chain retrovirus," *Cancer Res,* vol. 58, no. 23, pp. 5275-9, Dec 1 1998.

[23] I. Figueira *et al.*, "Picturing Breast Cancer Brain Metastasis Development to Unravel Molecular Players and Cellular Crosstalk," *Cancers (Basel),* vol. 13, no. 4, Feb 22 2021.

[24] Y. Chen *et al.*, "Glioma initiating cells contribute to malignant transformation of host glial cells during tumor tissue remodeling via PDGF signaling," *Cancer Lett,* vol. 365, no. 2, pp. 174-81, Sep 1 2015.

[25] M. Jechlinger *et al.*, "Autocrine PDGFR signaling promotes mammary cancer metastasis," *J Clin Invest,* vol. 116, no. 6, pp. 1561-70, Jun 2006.

[26] K. A. H. Thies, A.M.; Hildreth, B.E.; Steck, S.A.; Spehar, J.M.; Kladney, R.D.; Geisler, J.A.; Das, M.; Russell, L.O.; Bey, J.F.; et al. , "Stromal Platelet–Derived Growth Factor Receptor-β Signaling Promotes Breast Cancer Metastasis in the Brain. ," *Cancer Res.* , 2021.

[27] U. K. Westermark *et al.*, "RAD51 can inhibit PDGF-B-induced gliomagenesis and genomic instability," *Neuro Oncol,* vol. 13, no. 12, pp. 1277-87, Dec 2011.

[28] J. C. Wang *et al.*, "Metformin inhibits metastatic breast cancer progression and improves chemosensitivity by inducing vessel normalization via PDGF-B downregulation," *J Exp Clin Cancer Res,* vol. 38, no. 1, p. 235, Jun 4 2019.

[29] P. M. Costa *et al.*, "Tumor-targeted Chlorotoxin-coupled Nanoparticles for Nucleic Acid Delivery to Glioblastoma Cells: A Promising System for Glioblastoma Treatment," *Mol Ther Nucleic Acids,* vol. 2, p. e100, Jun 18 2013.

[30] L. C. Gomes-da-Silva *et al.*, "Toward a siRNA-containing nanoparticle targeted to breast cancer cells and the tumor microenvironment," *Int J Pharm,* vol. 434, no. 1-2, pp. 9-19, Sep 15 2012.

[31] J. P. W. Filipowicz, *Brenner's Encyclopedia of Genetics*, Second Edition ed. 2013.

[32] Ç. E. Jodi J. Speiser, Clodia Osipo, *Vitamins & Hormones*. 2013.

[33] M. Craig Shimasaki PhD, *Biotechnology Entrepreneurship (Leading, Managing and Commercializing Innovative Technologies)*, Second Edition ed. 2020.

[34] F. L. Cardoso, D. Brites, and M. A. Brito, "Looking at the blood-brain barrier: molecular anatomy and possible investigation approaches," *Brain Res Rev,* vol. 64, no. 2, pp. 328-63, Sep 24 2010.

[35] I. Figueira *et al.*, "MicroRNAs and Extracellular Vesicles as Distinctive Biomarkers of Precocious and Advanced Stages of Breast Cancer Brain Metastases Development," *Int J Mol Sci,* vol. 22, no. 10, May 14 2021.

[36] L. R. Tefas, C. Barbalata, C. Tefas, and I. Tomuta, "Salinomycin-Based Drug Delivery Systems: Overcoming the Hurdles in Cancer Therapy," *Pharmaceutics,* vol. 13, no. 8, Jul 22 2021.

[37] R. Banerjee, "Liposomes: applications in medicine," *J Biomater Appl,* vol. 16, no. 1, pp. 3-21, Jul 2001.

[38] T. M. Allen and P. R. Cullis, "Liposomal drug delivery systems: from concept to clinical applications," *Adv Drug Deliv Rev,* vol. 65, no. 1, pp. 36-48, Jan 2013.

[39] R. S. Shapiro, "COVID-19 vaccines and nanomedicine," *Int J Dermatol,* vol. 60, no. 9, pp. 1047-1052, Sep 2021.

[40] A. Jain, A. Tiwari, A. Verma, S. Saraf, and S. K. Jain, "Combination Cancer Therapy Using Multifunctional Liposomes," *Crit Rev Ther Drug Carrier Syst,* vol. 37, no. 2, pp. 105-134, 2020.

[41] S. C. Semple *et al.*, "Efficient encapsulation of antisense oligonucleotides in lipid vesicles using ionizable aminolipids: formation of novel small multilamellar vesicle structures," *Biochim Biophys Acta,* vol. 1510, no. 1-2, pp. 152-66, Feb 9 2001.

[42] T. M. Allen, C. Hansen, F. Martin, C. Redemann, and A. Yau-Young, "Liposomes containing synthetic lipid derivatives of poly(ethylene glycol) show prolonged circulation half-lives in vivo," *Biochim Biophys Acta,* vol. 1066, no. 1, pp. 29-36, Jul 1 1991.

[43] T. Coelho *et al.*, "Safety and efficacy of RNAi therapy for transthyretin amyloidosis," *N Engl J Med,* vol. 369, no. 9, pp. 819-29, Aug 29 2013.

[44] M. F. Coutinho *et al.*, "Lysosomal Storage Disease-Associated Neuropathy: Targeting Stable Nucleic Acid Lipid Particle (SNALP)-Formulated siRNAs to the Brain as a Therapeutic Approach," *Int J Mol Sci,* vol. 21, no. 16, Aug 10 2020.

[45] T. W. Geisbert *et al.*, "Postexposure protection of non-human primates against a lethal Ebola virus challenge with RNA interference: a proof-of-concept study," *Lancet,* vol. 375, no. 9729, pp. 1896-905, May 29 2010.

[46] D. V. Morrissey *et al.*, "Potent and persistent in vivo anti-HBV activity of chemically modified siRNAs," *Nat Biotechnol,* vol. 23, no. 8, pp. 1002-7, Aug 2005.

[47] T. S. Zimmermann *et al.*, "RNAi-mediated gene silencing in non-human primates," *Nature,* vol. 441, no. 7089, pp. 111-4, May 4 2006.

[48] A. D. Judge *et al.*, "Confirming the RNAi-mediated mechanism of action of siRNA-based cancer therapeutics in mice," *J Clin Invest,* vol. 119, no. 3, pp. 661-73, Mar 2009.

[49] M. T. Di Martino *et al.*, "In vivo activity of miR-34a mimics delivered by stable nucleic acid lipid particles (SNALPs) against multiple myeloma," *PLoS One,* vol. 9, no. 2, p. e90005, 2014.

[50] M. Conceicao *et al.*, "Intravenous administration of brain-targeted stable nucleic acid lipid particles alleviates Machado-Joseph disease neurological phenotype," *Biomaterials,* vol. 82, pp. 124-37, Mar 2016.

[51] J. Karlsson, K. M. Luly, S. Y. Tzeng, and J. J. Green, "Nanoparticle designs for delivery of nucleic acid therapeutics as brain cancer therapies," *Adv Drug Deliv Rev,* vol. 179, p. 113999, Dec 2021.

[52] S. Ayloo and C. Gu, "Transcytosis at the blood-brain barrier," *Curr Opin Neurobiol,* vol. 57, pp. 32-38, Aug 2019.

[53] B. Formicola *et al.*, "The synergistic effect of chlorotoxin-mApoE in boosting drug-loaded liposomes across the BBB," *J Nanobiotechnology,* vol. 17, no. 1, p. 115, Nov 11 2019.

[54] O. Cohen-Inbar and M. Zaaroor, "Glioblastoma multiforme targeted therapy: The Chlorotoxin story," *J Clin Neurosci,* vol. 33, pp. 52-58, Nov 2016.

[55] K. Wang *et al.*, "siRNA nanoparticle suppresses drug-resistant gene and prolongs survival in an orthotopic glioblastoma xenograft mouse model," *Adv Funct Mater,* vol. 31, no. 6, Feb 3 2021.

[56] C. Qin *et al.*, "Inhibition of metastatic tumor growth and metastasis via targeting metastatic breast cancer by chlorotoxin-modified liposomes," *Mol Pharm,* vol. 11, no. 10, pp. 3233-41, Oct 6 2014.

[57] P. G. Ojeda, C. K. Wang, and D. J. Craik, "Chlorotoxin: Structure, activity, and potential uses in cancer therapy," *Biopolymers,* vol. 106, no. 1, pp. 25-36, Jan 2016.

[58] A. N. Mamelak and D. B. Jacoby, "Targeted delivery of antitumoral therapy to glioma and other malignancies with synthetic chlorotoxin (TM-601)," *Expert Opin Drug Deliv,* vol. 4, no. 2, pp. 175-86, Mar 2007.

[59] L. Soroceanu, T. J. Manning, Jr., and H. Sontheimer, "Modulation of glioma cell migration and invasion using Cl(-) and K(+) ion channel blockers," *J Neurosci,* vol. 19, no. 14, pp. 5942-54, Jul 15 1999.

[60] J. Deshane, C. C. Garner, and H. Sontheimer, "Chlorotoxin inhibits glioma cell invasion via matrix metalloproteinase-2," *J Biol Chem,* vol. 278, no. 6, pp. 4135-44, Feb 7 2003.

[61] M. J. Duffy, T. M. Maguire, A. Hill, E. McDermott, and N. O'Higgins, "Metalloproteinases: role in breast carcinogenesis, invasion and metastasis," *Breast Cancer Res,* vol. 2, no. 4, pp. 252-7, 2000.

[62] J. Dewangan, S. Srivastava, and S. K. Rath, "Salinomycin: A new paradigm in cancer therapy," *Tumour Biol,* vol. 39, no. 3, p. 1010428317695035, Mar 2017.

[63] D. Fuchs, A. Heinold, G. Opelz, V. Daniel, and C. Naujokat, "Salinomycin induces apoptosis and overcomes apoptosis resistance in human cancer cells," *Biochem Biophys Res Commun,* vol. 390, no. 3, pp. 743-9, Dec 18 2009.

[64] A. Huczynski, J. Janczak, M. Antoszczak, J. Wietrzyk, E. Maj, and B. Brzezinski, "Antiproliferative activity of salinomycin and its derivatives," *Bioorg Med Chem Lett,* vol. 22, no. 23, pp. 7146-50, Dec 1 2012.

[65] K. Ketola *et al.*, "Salinomycin inhibits prostate cancer growth and migration via induction of oxidative stress," *Br J Cancer,* vol. 106, no. 1, pp. 99-106, Jan 3 2012.

[66] H. J. Choi, Kim, K. Y., Yu, S. N., Kim, S. H., Chun, S. S., Yu, H. S., ... & Ahn, S. C. , "Salinomycin-induced apoptosis in human prostate cancer cells," *In Advances in Prostate Cancer,* 2013.

[67] F. Wang *et al.*, "Salinomycin inhibits proliferation and induces apoptosis of human hepatocellular carcinoma cells in vitro and in vivo," *PLoS One,* vol. 7, no. 12, p. e50638, 2012.

[68] J. R. Jangamreddy *et al.*, "Salinomycin induces activation of autophagy, mitophagy and affects mitochondrial polarity: differences between primary and cancer cells," *Biochim Biophys Acta,* vol. 1833, no. 9, pp. 2057-69, Sep 2013.

[69] J. V. McCarthy and T. G. Cotter, "Cell shrinkage and apoptosis: a role for potassium and sodium ion efflux," *Cell Death Differ,* vol. 4, no. 8, pp. 756-70, Dec 1997.

[70] C. Naujokat and R. Steinhart, "Salinomycin as a drug for targeting human cancer stem cells," *J Biomed Biotechnol,* vol. 2012, p. 950658, 2012.

[71] H. An, J. Y. Kim, E. Oh, N. Lee, Y. Cho, and J. H. Seo, "Salinomycin Promotes Anoikis and Decreases the CD44+/CD24- Stem-Like Population via Inhibition of STAT3 Activation in MDA-MB-231 Cells," *PLoS One,* vol. 10, no. 11, p. e0141919, 2015.

[72] J. H. Kim *et al.*, "Salinomycin sensitizes cancer cells to the effects of doxorubicin and etoposide treatment by increasing DNA damage and reducing p21 protein," *Br J Pharmacol,* vol. 162, no. 3, pp. 773-84, Feb 2011.

[73] Y. Al Dhaheri *et al.*, "Salinomycin induces apoptosis and senescence in breast cancer: upregulation of p21, downregulation of survivin and histone H3 and H4 hyperacetylation," *Biochim Biophys Acta,* vol. 1830, no. 4, pp. 3121-35, Apr 2013.

[74] A. M. Niwa *et al.*, "Salinomycin efficiency assessment in non-tumor (HB4a) and tumor (MCF-7) human breast cells," *Naunyn Schmiedebergs Arch Pharmacol,* vol. 389, no. 6, pp. 557-71, Jun 2016.

[75] P. B. Gupta *et al.*, "Identification of selective inhibitors of cancer stem cells by high-throughput screening," *Cell,* vol. 138, no. 4, pp. 645-659, Aug 21 2009.

[76] Y. J. Kim *et al.*, "Co-Eradication of Breast Cancer Cells and Cancer Stem Cells by Cross-Linked Multilamellar Liposomes Enhances Tumor Treatment," *Mol Pharm,* vol. 12, no. 8, pp. 2811-22, Aug 3 2015.

[77] Z. Gong *et al.*, "Codelivery of salinomycin and doxorubicin using nanoliposomes for targeting both liver cancer cells and cancer stem cells," *Nanomedicine (Lond),* vol. 11, no. 19, pp. 2565-2579, Oct 2016.

[78] F. Xie *et al.*, "Codelivery of salinomycin and chloroquine by liposomes enables synergistic antitumor activity in vitro," *Nanomedicine (Lond),* vol. 11, no. 14, pp. 1831-46, Jul 2016.

[79] D. Momekova *et al.*, "Sterically stabilized liposomes as a platform for salinomycin metal coordination compounds: physicochemical characterization and in vitro evaluation," *Journal of Drug Delivery Science and Technology,* vol. 23 no. 3, pp. 215-223, 2013.

[80] Kirby C. and G. G., "Dehydration-rehydration vesicles: a simple method for high yield drug entrapment in liposomes," *Bio/Technology* vol. 2, no. 11, pp. 979-984, 1984.

[81] L. S. Mendonça, F. Firmino, J. N. Moreira, M. C. P. d. Lima, and S. Simões, "Transferrin Receptor-Targeted Liposomes Encapsulating anti-BCR-ABL siRNA or asODN for Chronic Myeloid Leukemia Treatment," *Bioconjugate Chem,* vol. 21, no. 1, pp. 157-168, 2010.

[82] A. T. Ness, J. V. Pastewka, and A. C. Peacock, "Evaluation of a Recently Reported Stable Liebermann-Burchard Reagent and Its Use for the Direct Determination of Serum Total Cholesterol," *Clin Chim Acta,* vol. 10, pp. 229-37, Sep 1964.

[83] G. Rouser, Fleischer, S. & Yamamoto, A, "Two dimensional thin layer chromatographic separation of polar lipids and determination of phospholipids by phosphorus analysis of spots.," *Lipids Health Dis,* vol. 5, pp. 496-496, 1970.

[84] J. Godinho-Pereira, A. R. Garcia, I. Figueira, R. Malho, and M. A. Brito, "Behind Brain Metastases Formation: Cellular and Molecular Alterations and Blood-Brain Barrier Disruption," *Int J Mol Sci,* vol. 22, no. 13, Jun 30 2021.

[85] B. Srinivasan, A. R. Kolli, M. B. Esch, H. E. Abaci, M. L. Shuler, and J. J. Hickman, "TEER measurement techniques for in vitro barrier model systems," *J Lab Autom,* vol. 20, no. 2, pp. 107-26, Apr 2015.

[86] I. Figueira *et al.*, "Polyphenols journey through blood-brain barrier towards neuronal protection," *Sci Rep,* vol. 7, no. 1, p. 11456, Sep 13 2017.

[87] M. L. Briuglia, C. Rotella, A. McFarlane, and D. A. Lamprou, "Influence of cholesterol on liposome stability and on in vitro drug release," *Drug Deliv Transl Res,* vol. 5, no. 3, pp. 231-42, Jun 2015.

[88] H. Rayess, M. B. Wang, and E. S. Srivatsan, "Cellular senescence and tumor suppressor gene p16," *Int J Cancer,* vol. 130, no. 8, pp. 1715-25, Apr 15 2012.

[89] I. Palmela *et al.*, "Time-dependent dual effects of high levels of unconjugated bilirubin on the human blood-brain barrier lining," *Front Cell Neurosci,* vol. 6, p. 22, 2012.

[90] B. H. Nam *et al.*, "Breast cancer subtypes and survival in patients with brain metastases," *Breast Cancer Res,* vol. 10, no. 1, p. R20, 2008.

[91] R. Narayanaswamy and V. P. Torchilin, "Targeted Delivery of Combination Therapeutics Using Monoclonal Antibody 2C5-Modified Immunoliposomes for Cancer Therapy," *Pharm Res,* vol. 38, no. 3, pp. 429-450, Mar 2021.

[92] J. Y. Zhang *et al.*, "Regulating Stem Cell-Related Genes Induces the Plastic Differentiation of Cancer Stem Cells to Treat Breast Cancer," *Mol Ther Oncolytics,* vol. 18, pp. 396-408, Sep 25 2020.

[93] D. Drabik, G. Chodaczek, S. Kraszewski, and M. Langner, "Mechanical Properties Determination of DMPC, DPPC, DSPC, and HSPC Solid-Ordered Bilayers," *Langmuir,* vol. 36, no. 14, pp. 3826-3835, Apr 14 2020.

[94] D. Papahadjopoulos *et al.*, "Sterically Stabilized Liposomes: Improvements in Pharmacokinetics and Antitumor Therapeutic Efficacy " *National Academy of Sciences,* vol. 88, no. 24, pp. 11460-11464, 1991.

[95] W. W. Sułkowski, D. Pentak, K. Nowak, and A. Sułkowska, "The influence of temperature, cholesterol content and pH on liposome stability," *Journal of Molecular Structure,* vol. 744-747, pp. 737-347, 2005.

[96] S. G. Antimisiaris, "Preparation of DRV Liposomes," *Methods Mol Biol,* vol. 1522, pp. 23-47, 2017.

[97] M. Kai *et al.*, "Targeting breast cancer stem cells in triple-negative breast cancer using a combination of LBH589 and salinomycin," *Breast Cancer Res Treat,* vol. 151, no. 2, pp. 281-94, Jun 2015.

[98] S. Zhou *et al.*, "Salinomycin Suppresses PDGFRbeta, MYC, and Notch Signaling in Human Medulloblastoma," *Austin J Pharmacol Ther,* vol. 2, no. 3, p. 1020, 2014.

[99] T. Alqahtani, V. M. Kumarasamy, A. Huczynski, and D. Sun, "Salinomycin and its derivatives as potent RET transcriptional inhibitors for the treatment of medullary thyroid carcinoma," *Int J Oncol,* vol. 56, no. 1, pp. 348-358, Jan 2020.

[100] A. M. Niwa, S. C. Semprebon, G. F. R. D'Epiro, L. A. Marques, T. A. Zanetti, and M. S. Mantovani, "Salinomycin induces cell cycle arrest and apoptosis and modulates hepatic cytochrome P450 mRNA expression in HepG2/C3a cells," *Toxicol Mech Methods,* vol. 32, no. 5, pp. 341-351, Jun 2022.

[101] D. Papahadjopoulos *et al.*, "Sterically stabilized liposomes: improvements in pharmacokinetics and antitumor therapeutic efficacy," *Proc Natl Acad Sci U S A,* vol. 88, no. 24, pp. 11460-4, Dec 15 1991.

[102] S. D. Allison, "Liposomal drug delivery," *J Infus Nurs,* vol. 30, no. 2, pp. 89-95; quiz 120, Mar-Apr 2007.

[103] A. Karimian, Y. Ahmadi, and B. Yousefi, "Multiple functions of p21 in cell cycle, apoptosis and transcriptional regulation after DNA damage," *DNA Repair (Amst),* vol. 42, pp. 63-71, Jun 2016.

[104] C. Artus *et al.*, "The Wnt/planar cell polarity signaling pathway contributes to the integrity of tight junctions in brain endothelial cells," *J Cereb Blood Flow Metab,* vol. 34, no. 3, pp. 433-40, Mar 2014.

[105] R. T. Moon, "Wnt/β-Catenin Pathway," *SCIENCE'S STKE,* vol. 2005, no. 271, 2005.

[106] H. Li *et al.*, "LncRNA MALAT1 modulates ox-LDL induced EndMT through the Wnt/beta-catenin signaling pathway," *Lipids Health Dis,* vol. 18, no. 1, p. 62, Mar 14 2019.

[107] H. R. Wardill *et al.*, "Cytokine-mediated blood brain barrier disruption as a conduit for cancer/chemotherapy-associated neurotoxicity and cognitive dysfunction," *Int J Cancer,* vol. 139, no. 12, pp. 2635-2645, Dec 15 2016.

[108] F. Marcucci, A. Corti, and A. J. M. Ferreri, "Breaching the Blood-Brain Tumor Barrier for Tumor Therapy," *Cancers (Basel),* vol. 13, no. 10, May 15 2021.

[109] K. Mitusova, O. O. Peltek, T. E. Karpov, A. R. Muslimov, M. V. Zyuzin, and A. S. Timin, "Overcoming the blood-brain barrier for the therapy of malignant brain tumor: current status and prospects of drug delivery approaches," *J Nanobiotechnology,* vol. 20, no. 1, p. 412, Sep 15 2022.

VIII. Supplementary Material

8.1 Example of Salinomycin report

SERVIÇO LC-MS **DATA: 2022.07.04**

Tipo de Análise

MS ☐ MS/MS ☐ LC-MS ☐ LC-MS/MS ☑

Dados do Requisitante

Nome: Joana Godinho Pereira; Joana Romão; Prof. Alexandra Brito

Contacto: joanagpereira@ff.ulisboa.pt; joana.romao@live.com.pt; abrito@ff.ulisboa.pt

Informação de Serviço

Data de Entrega da(s) Amostra(s): 28 junho 2022

Data da Análise: 30 junho – 1 julho 2022

Relatório: 04 julho 2022

Técnico: Andreia Bento da Silva

Resumo

- Procedeu-se à quantificação de salinomicina de sódio (SAL) na amostra, por UHPLC-MS/MS. Os resultados (médias) encontram-se descritos na **Tabela 3**, página 3.
- As condições de análise encontram-se descritas nos **ANEXOS 1 e 2**.
- A amostra foi preparada de acordo com o descrito no **ANEXO 3**.
- A quantificação de SAL foi determinada de acordo com o descrito nos **ANEXOS 4 e 5**.

Lisboa, 04 de julho de 2022

Elaborado por:

BentoSilva

(Andreia Bento da Silva)

Conteúdo

1. Amostragem e Análise

- Foram entregues no Laboratório de Análise Estrutural (LAE):
  1. Padrão de salinomicina de sódio (SAL), descrito na **Tabela 1** (em dezembro de 2021);
  2. Amostras de formulação de SAL [**Tabela 2**].
- A solução de SAL a 1 mg mL^{-1} foi mantida a -20 °C e as amostras foram mantidas a 4 °C até ao dia da análise.

Tabela 1. Descrição do padrão entregue no LAE.

Composto	Concentração (mg mL^{-1})	Solvente	Massa monoisotópica	Fórmula Molecular	Estrutura Molecular
Salinomicina de sódio (SAL)	1.0	Acetonitrilo	772	$C_{42}H_{69}NaO_{11}$	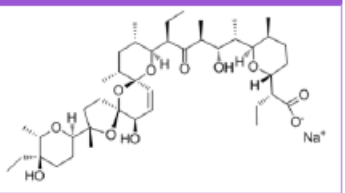

Tabela 2. Descrição das amostras a analisar.

Amostra	Descrição da formulação	Solvente	Concentração teórica máxima de SAL (µg mL^{-1})
EPC-Sal (final)	EPC:DSPE-PEG:CTX (9.5:0.4:0.04)	Hepes NaCl pH 7.4	3865

2. Resultados

- A concentração de SAL na amostra encontra-se descrita na **Tabela 3**.

Tabela 3. Concentração de SAL na amostra.

Amostra	Concentração teórica máxima (µg mL^{-1} amostra)	Concentração (µg mL^{-1} amostra)
EPC-Sal (final)	3865	638 ± 49

ANEXO 1. Equipamento

Utilizou-se um equipamento de cromatografia líquida (UHPLC) modelo Waters Acquity™ Ultra Performance LC (Waters®, Ireland) que consiste num sistema de bombas binárias, desgaseificador, amostrador automático e fornopara coluna. O espectrómetro de massa utilizado foi do tipo triplo quadrupolo, modelo Waters Acquity™ (Waters®, Ireland). As condições de MS/MS (voltagem de cone, energia de colisão, etc.) foram otimizadas para a quantificação de salinomicina de sódio (SAL). As amostras foram analisadas em modo MRM (*multiple reaction monitoring*), de modo a melhorar a seletividade e sensibilidade. Foram usadas duas transições para quantificar (MRM 1) e confirmar a identificação (MRM 2) de SAL, com um desvio máximo de 30% entre a razão MRM1/MRM2 (*ion ratio*). Para aquisição e processamento de dados utilizou-se o software MassLynx® versão 4.1.

ANEXO 2. Condições de análise (UHPLC-MS/MS)

2.1 Condições do método cromatográfico (UHPLC)

Coluna	Purospher® STAR RP-18 2µm (2.1 x 50 mm)
Eluentes:	
A	0.1% HCOOH em água
B	Acetonitrilo
Fluxo (mL min^{-1})	0.3
Tempo Total (mins)	10
Temperatura da Coluna (°C)	35
Volume de Injeção (µL)	10 µL

Método de UHPLC:

Tempo (min)	A%	B%
0	20.0	80.0
1	20.0	80.0
5	5.0	95.0
7	5.0	95.0
7.1	20.0	80.0
10	20.0	80.0

2.2 Condições de ionização e fragmentação (MS/MS)

Polaridade	ES+
Capilar (kV)	3.00
Extrator (V)	1.00
Lente RF (V)	0.1
Temperatura da Fonte (°C)	120
Temperatura de Dessolvatação (°C)	350
Fluxo do Gás do Cone (L/Hr)	50
Fluxo do Gás de Dessolvatação (L/Hr)	750

A quantificação de salinomicina de sódio (SAL) foi obtida em modo "MRM" para as transições:

SAL (ESI+):

Reação em cadeia	*Dwell* (seg)	Volt. Cone (V)	Energia de Colisão (eV)
MRM 1: 773.00 > 431.00	0.242	60.0	40.0
MRM 2: 773.00 > 531.00	0.242	60.0	40.0

ANEXO 3. Extração de salinomicina de sódio da formulação

1. Retiraram-se 10 µL de amostra e adicionaram-se 990 µL de ACN (diluição 1:100);
2. A solução foi agitada no vórtex, 10 segundos;
3. Levou-se a solução a um banho de ultrassons, 10 minutos;
4. A solução fora filtrada por filtro de PTFE 0.20 µm;
5. A solução foi diluída em ACN (1:10 000), de modo a obter uma diluição final de 1:1 000 000, e posteriormenteinjetada no equipamento.
6. A amostra foi preparada em quadruplicado.

ANEXO 4. Curvas de calibração

- Uma vez que não se verificaram efeitos de matriz significativos (relatório do pedido de análise 585/2021), aamostra foi quantificada através de uma curva de calibração em solvente (ACN) [**Tabela 4** e **Figura 1**].
- A média do *ion ratio* (razão das áreas dos picos MRM1/MRM2) obtida com a injeção dos padrões de SAL foi de 1.4 ± 0.06. Este valor foi usado para cálculo do desvio do *ion ratio* de SAL na amostra.

Tabela 4. Curvas de calibração de SAL.

Conc.: concentração de SAL (ng mL^{-1}); **TR:** tempo de retenção (minutos); **IR**: *ion ratio*.

Conc. teórica	TR	Área	Conc. calculada	Desvio conc. (%)	IR	Desvio IR (%)
0.1	3.44	64	0.11	5	1.3	-6
0.2	3.44	141	0.20	2	1.3	-6
0.3	3.45	224	0.29	2	1.4	1
0.4	3.44	287	0.37	8	1.4	1
0.5	3.43	427	0.53	6	1.5	9
0.6	3.43	476	0.59	2	1.4	1
0.7	3.43	598	0.73	5	1.4	1
0.8	3.43	652	0.80	0	1.4	1
0.9	3.42	746	0.91	1	1.3	-6
1.0	3.43	804	0.98	2	1.4	1

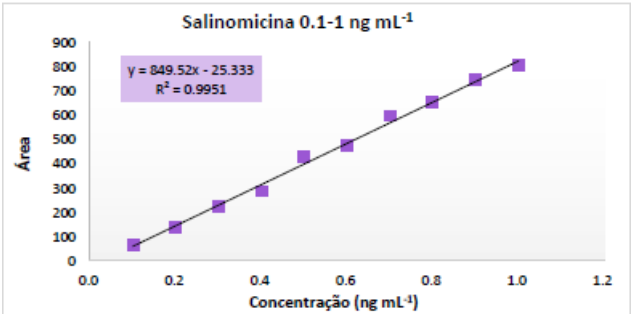

Figura 1. Curva de calibração de SAL em solvente (ACN).

ANEXO 5. Quantificação de salinomicina de sódio

- A amostra foi preparada de acordo com o **ANEXO 3**.
- Procedeu-se à quantificação de SAL na amostra [**Tabela 5**], considerando a equação da reta descrita no **ANEXO 4** (*y = 849.52 x - 25.333*).
- Os desvios obtidos para o *ion ratio* foram inferiores a 30% [**Tabela 5**], confirmando a presença de SAL na amostra.
- Os perfis cromatográficos obtidos para os quadruplicados encontram-se representados na **Figura 2**.

Tabela 5. Quantificação de SAL nos quadruplicados da amostra.

Conc.: concentração de SAL; **TR:** tempo de retenção (minutos); **FD**: fator de diluição; **IR**: *ion ratio*; **DP**: desvio padrão; **CV**: coeficiente de variação. **Conc. média** e **DP** expressos em µg mL^{-1}.

Sample Text	RT	IR	Desvio IR (%)	Área	Conc. (ng mL^{-1})	Conc. x FD (µg mL^{-1})	Conc. média	DP	CV (%)
Final (1)	3.41	1.4	1.4	492	0.61	609	638	49	7.7
Final (2)	3.41	1.5	8.7	485	0.60	601			
Final (3)	3.41	1.5	8.7	513	0.63	634			
Final (4)	3.40	1.4	1.4	577	0.71	709			

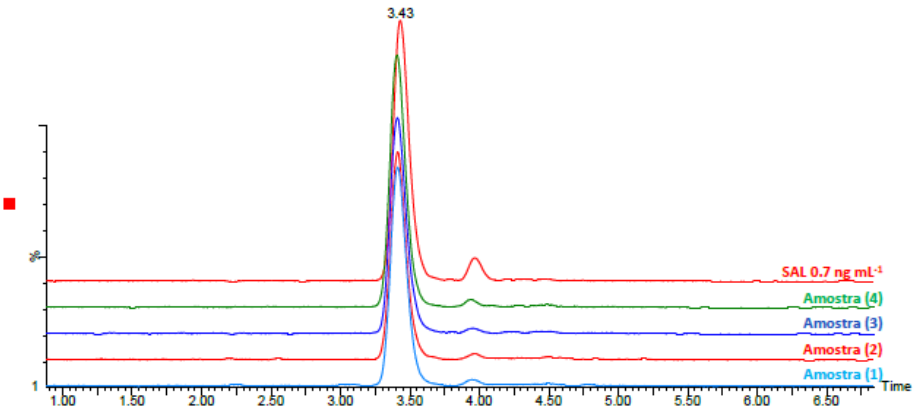

Figura 2. Comparação dos perfis cromatográficos adquiridos por TIC (*total ion chromatogram*) MRM dos quadruplicados da amostra e padrão de SAL 0.7 ng mL^{-1}.